



HAL
open science

Functional reconstitution of the type IVa pilus assembly system from enterohaemorrhagic *Escherichia coli*.

Areli Luna Rico, Weili Zheng, Nathalie Petiot, Edward H Egelman, Olivera Francetic

► To cite this version:

Areli Luna Rico, Weili Zheng, Nathalie Petiot, Edward H Egelman, Olivera Francetic. Functional reconstitution of the type IVa pilus assembly system from enterohaemorrhagic *Escherichia coli*. *Molecular Microbiology*, 2019, 111 (3), pp.732-749. 10.1111/mmi.14188 . pasteur-02282169

HAL Id: pasteur-02282169

<https://pasteur.hal.science/pasteur-02282169>

Submitted on 9 Sep 2019

HAL is a multi-disciplinary open access archive for the deposit and dissemination of scientific research documents, whether they are published or not. The documents may come from teaching and research institutions in France or abroad, or from public or private research centers.

L'archive ouverte pluridisciplinaire **HAL**, est destinée au dépôt et à la diffusion de documents scientifiques de niveau recherche, publiés ou non, émanant des établissements d'enseignement et de recherche français ou étrangers, des laboratoires publics ou privés.

1 Functional reconstitution of the type IVa pilus assembly system from enterohaemorrhagic
2 *Escherichia coli*

3

4 Running title: Reconstitution of type 4 pilus assembly system in *E. coli*

5

6 Areli Luna Rico^{1,2}, Weili Zheng³, Nathalie Petiot¹, Edward H. Egelman³ and Olivera

7 Francetic¹

8 ¹Biochemistry of Macromolecular Interactions Unit, Department of Structural Biology and
9 Chemistry, Institut Pasteur, CNRS UMR3528, 28 rue du Dr Roux, 75724 Paris, France.

10 ²Structural Bioinformatics Unit and NMR of Biomolecules Unit, Department of Structural
11 Biology and Chemistry, Institut Pasteur, CNRS UMR3528, 28 rue du Dr Roux, 75724 Paris,
12 France

13 ³Department of Biochemistry and Molecular Genetics, University of Virginia, Charlottesville,
14 VA22908, USA

15

16

17 Key words: type 4 pili, EHEC O157:H7, electron microscopy, type 2 secretion system,

18 Gibson assembly, bacterial two-hybrid, Sxy, type 4 filaments

19

20 **Summary**

21 Type 4a pili (T4aP) are long, thin and dynamic fibres displayed on the surface of diverse

22 bacteria promoting adherence, motility and transport functions. Genomes of many

23 Enterobacteriaceae contain conserved gene clusters encoding putative T4aP assembly

24 systems. However, their expression has been observed only in few strains including

25 Enterohaemorrhagic *Escherichia coli* (EHEC) and their inducers remain unknown. Here we

26 used EHEC genomic DNA as template to amplify and assemble an artificial operon

27 composed of four gene clusters encoding 13 pilus assembly proteins. Controlled expression

28 of this operon in non-pathogenic *E. coli* strains led to efficient assembly of T4aP composed

29 of the major pilin PpdD, as shown by shearing assays and immuno-fluorescence microscopy.

30 When compared with PpdD pili assembled in a heterologous *Klebsiella* T2SS type 2

31 secretion system (T2SS) by using cryo-electron microscopy (cryoEM), these pili showed
32 indistinguishable helical parameters, emphasizing that major pilins are the principal
33 determinants of fibre structure. Bacterial two-hybrid analysis identified several interactions of
34 PpdD with T4aP assembly proteins, and with components of the T2SS that allow for
35 heterologous fibre assembly. These studies lay ground for further characterization of T4aP
36 structure, function and biogenesis in enterobacteria.

37

38 **Introduction**

39

40 Pili or fimbriae are hair-like appendages that decorate the surface of many bacteria and allow
41 them to adhere to biotic or abiotic substrates. Among the prokaryotic surface structures, T4P
42 are arguably the most widespread and ancient, sharing common evolutionary origins with
43 archaeal flagella and pili (Makarova *et al.*, 2016). Together with bacterial T2SSs, they are
44 members of the type 4 filament (Tff) superfamily of structurally and functionally related
45 prokaryotic nanomachines (Berry & Pelicic, 2015). T4P are present in Gram-positive and
46 Gram-negative bacteria (Berry & Pelicic, 2015, Melville & Craig, 2013, Hospenthal *et al.*,
47 2017). They can be grouped into three main subtypes, a, b and c (or Tad pili), which share
48 common assembly pathway while showing differences in subunit primary sequence,
49 assembly components, and gene organization (Tomich *et al.*, 2007, Pelicic, 2008, Ellison *et*
50 *al.*, 2017). While the genes encoding T4b and T4c pili are typically clustered in a single
51 operon, those encoding T4aP are split in several gene clusters localized in conserved
52 positions around the bacterial chromosome (Pelicic, 2008).

53 T4P are mainly built as helical homo-polymers of a single subunit called the major
54 pilin. In addition, one or several minor pilin subunits might participate in assembly, priming
55 the initiation, modulating fibre dynamics or surface epitopes (Helaine *et al.*, 2007, Berry *et al.*,
56 2016, Cehovin *et al.*, 2013, Nguyen *et al.*, 2015, Ng *et al.*, 2016). Pilins are initially inserted in
57 the plasma membrane as precursors containing an N-terminal positively charged cytoplasmic
58 leader peptide acting as a membrane anchor. A dedicated prepilin peptidase PilD removes

59 this peptide and N-methylates mature pilins to allow for their membrane extraction and
60 incorporation at the base of the growing pilus (Strom & Lory, 1991, Strom *et al.*, 1993,
61 Santos-Moreno *et al.*, 2017).

62 Composition and function of T4aP assembly machinery have been extensively
63 characterized in several model organisms, including *Pseudomonas* and *Neisseria* (Leighton
64 *et al.*, 2015a, Berry & Pelicic, 2015). The T4a pilus systems (T4aPS), depicted schematically
65 in Fig. 1A, comprise four sub-complexes: the cytoplasmic ATPase motor complex, the inner-
66 membrane (IM)- anchored assembly platform (AP) complex, the outer-membrane (OM)
67 secretin complex (exclusively in Gram-negative bacteria), and the filament (Chang *et al.*,
68 2016, Gold *et al.*, 2015). The ATPase motor PilB (according to the *P. aeruginosa*
69 nomenclature) localized at the base of the system, powers pilus assembly (Karuppiah *et al.*,
70 2013, Tammam *et al.*, 2013, McCallum *et al.*, 2017). PilB interacts with the platform protein
71 PilC and with the PilM component of the IM complex that also includes PilN and PilO (Ayers
72 *et al.*, 2009, Georgiadou *et al.*, 2012). The IM AP complex is connected *via* PilP to the OM
73 secretin channel formed by the PilQ multimer (Koo *et al.*, 2016) that allows pilus exposure on
74 the bacterial surface (Wolfgang *et al.*, 1998). The major pilins in *P. aeruginosa* (Tammam *et al.*
75 *et al.*, 2013) and *Neisseria* (Georgiadou *et al.*, 2012) interact with the AP, which presumably
76 transmits conformational changes in PilB to promote pilin polymerization. AP components
77 also orchestrate pilus retraction, powered by the PilT ATPase (Misic *et al.*, 2010, Leighton *et al.*
78 *et al.*, 2015b). Recently, cryo-electron microscopy brought more detailed insights into several
79 T4aP structures (Kolappan *et al.*, 2016, Wang *et al.*, 2017), while advances in cryo-electron
80 tomography revealed global organization of T4aP assembly systems *in situ*, in the envelope
81 of *Pseudomonas* (Gold *et al.*, 2015) and *Myxococcus* (Chang *et al.*, 2016).

82
83 The *Escherichia coli* chromosome harbours genes that encode all components of a
84 putative T4aP assembly system, similar to the well-studied systems in *P. aeruginosa* and
85 *Neisseria* spp. The promoter regions of predicted T4aP operons in *E. coli* contain binding
86 motifs called CRP-S, reminiscent of the catabolic repressor protein (CRP) binding sites

87 (Cameron & Redfield, 2006). These CRP-S motifs are low-affinity binding sites for the
88 catalytic repressor protein (CRP) that require cAMP and the natural competence activator
89 Sxy (or TfoX) to allow for transcriptional activation of downstream genes (Cameron &
90 Redfield, 2006). The presence of these sites upstream of T4aP and DNA uptake genes
91 suggests that, like *Pasteurellaceae* and *Vibrionaceae*, *E. coli* and other enterobacteria have
92 the genetic potential for natural competence (Cameron & Redfield, 2006). Indeed, Sxy
93 overproduction in *E. coli* activates transcription of *ppd/hof* operons encoding T4P, but also
94 that of genes encoding the DNA uptake machinery (Sinha *et al.*, 2009). Moreover, *sxy*
95 expression can promote uptake of external DNA (Sinha & Redfield, 2012), supporting the
96 role of T4aP in natural competence. In *E. coli* K-12 *sxy* expression is auto-regulated in a
97 CRP-cAMP dependent manner and activated by the stress sigma factor RpoS (Jaskolska &
98 Gerdes, 2015). However transcriptional analyses show that T4P genes are silent in *E. coli* K-
99 12 under a variety of conditions tested (Sauvonnet *et al.*, 2000a, Sinha *et al.*, 2009) and
100 specific signals and conditions that induce Sxy production in *E. coli* remain unknown.

101 The first indication that *ppd/hof* genes may encode a functional system has come
102 from studies of enterohaemorrhagic *E. coli* (EHEC), which produce pili composed of the
103 major subunit PpdD in minimal casein medium (Xicohtencatl-Cortes *et al.*, 2007). EHEC is a
104 major intestinal pathogen causing haemorrhagic colitis and haemolytic uremic syndrome
105 (HUS), associated with significant mortality and morbidity (Monteiro *et al.*, 2016). Sera of
106 patients recovering from HUS contain PpdD-reactive antibodies (Xicohtencatl-Cortes *et al.*,
107 2007). Ectopic expression of the plasmid-borne *ppdD-hofBC* operon conferred to an *E. coli*
108 strain HB101 several T4P-linked phenotypes, including adherence and twitching motility
109 (Xicohtencatl-Cortes *et al.*, 2009). Importantly, PpdD pili (also designated HCP, for
110 hemorrhagic coli pili) contribute to EHEC adherence to intestinal tissues (Xicohtencatl-Cortes
111 *et al.*, 2007) and induce pro-inflammatory signalling (Ledesma *et al.*, 2010).

112 In view of this functional evidence, here we used the *ppd/hof* genes from the EHEC
113 strain EDL933 as building blocks to reconstitute an artificial T4P assembly operon in non-
114 pathogenic *E. coli*. Successful reconstitution of pilus assembly in this system allowed us to

115 compare PpdD fibres polymerized by the cognate T4aPS to those produced when PpdD is
116 assembled by the heterologous T2SS of *Klebsiella oxytoca* (Sauvonnet *et al.*, 2000b,
117 Cisneros *et al.*, 2012b). Despite different PpdD interactions with the assembly components of
118 these systems, the resulting pili are highly similar, consistent with the role of major pilins as
119 key determinants of the fibre symmetry.

120

121 **Results**

122

123 *Enterobacterial T4aP assembly systems share common features*

124

125 Genes that encode T4aP assembly systems in *E. coli* and other enterobacterial
126 genera are found in conserved chromosomal loci (Fig. 1), as highlighted previously (Pelicic,
127 2008). The *ppdD-hofBC* operon encoding the major pilin, the ATPase HofB and the platform
128 protein HofC is localised between *guaC* and *ampD* genes at 3 min of the *E. coli* map (genes
129 Z0116-0118 in EHEC strain EDL933) (Perna *et al.*, 2001). At min 61, between the *thyA* and
130 *recC* genes, the *ppdAB-ygdB-ppdC* operon encodes the four minor pilins. The *hofMNOPQ*
131 operon encodes the assembly platform complex connecting HofB ATPase with the secretin
132 HofQ and is located at min 75 between *aroK* and *mrcA* genes (Fig. 1B). The *yggR* gene
133 encoding a PilT homologue is localized at min 66 (not depicted) and corresponds to Z4295
134 gene in EHEC. In *Pseudomonas* and *Vibrio* genomes the essential prepilin peptidase gene
135 *pilD* is linked to the major pilin operon *pilABCD* (Fullner & Mekalanos, 1999). This is not the
136 case in Enterobacteriaceae, where *pilD* homologues are linked to operons encoding T2SSs.
137 The gene *gspO*, one of the two prepilin peptidase genes in *E. coli* K-12, is the last gene of
138 the *gsp* operon encoding the chitinase-specific T2SS (Francetic *et al.*, 1998, Francetic *et al.*,
139 2000). In EHEC, almost all *gsp* genes have been lost during evolution, leaving only the *gspO*
140 fragment encoding the prepilin peptidase catalytic domain (gene Z4693) (Perna *et al.*, 2001).
141 Additionally, EHEC strains have the *gspO* homologue *etpO* within a plasmid-encoded T2SS
142 cluster (Schmidt *et al.*, 1997).

143 The genes encoding the major T4a pilins are remarkably conserved in all *E. coli*
144 strains sequenced to date (Fig. 2). A single amino acid difference is found between the
145 primary sequence of the major pilin PpdD from *E. coli* K-12 and EHEC. Furthermore, there is
146 a high sequence similarity between the EHEC PpdD and major pilins from diverse genera of
147 the Enterobacteriaceae family, including *Salmonella* (88.4% of identical residues), *Yersinia*
148 (58.2%), *Shigella* (97.3%), *Raoultella* (82.9%), *Dickeya* (60.1%), *Serratia* (59.2%), *Proteus*
149 (42.1%), *Citrobacter* (89.7%), *Klebsiella* (86.3%), or *Pantoea* (60.1%) (Fig. 2A and Fig. S1).
150 Compared to well-studied major pilins, PilE of *Neisseria* and PilA of *Pseudomonas*, which
151 contain two cysteine residues near their C-terminus forming a disulphide bond (Fig. 2B)
152 (Parge *et al.*, 1995, Craig *et al.*, 2003), PpdD and its homologues contain an additional pair
153 of Cys residues at positions 50 and 60. In PpdD, NMR and chemical shift analysis showed
154 that these residues form disulphide bonds, one at the junction between the long α -helical
155 stem and the globular domain, and the second close to the C-terminus defining the variable
156 D loop typically found in T4a pilins (de Amorim *et al.*, 2014). These residues are fully
157 conserved in all PpdD homologues (Fig. 2A), suggesting that major pilins in
158 Enterobacteraceae share a similar structure. Like PpdD, the minor pilins PpdA, PpdB, YgdB
159 and PpdC and their homologues in the family contain two conserved Cys pairs at similar
160 positions.

161

162

163 *Assembly of the artificial ppd-hof operon*

164

165 Since the EHEC strain EDL933 assembles functional pili (Xicohtencatl-Cortes *et al.*,
166 2007), we used its genomic DNA as template to PCR-amplify the *ppdD-hofB-hofC*, *ppdAB-*
167 *ygdB-ppdC* and *hofMNOPQ* clusters, flanked with ~100 bp of noncoding DNA. We amplified
168 a pBR322-derived vector fragment carrying the replication origin and the Ap^R selection
169 marker and used the Gibson assembly approach (Gibson *et al.*, 2009) to join these PCR
170 products into a plasmid named pMS10 (Table 2). To complete the artificial operon, we

171 introduced at its distal end the *gspO* gene, PCR-amplified from *E. coli* K-12 strain MG1655,
172 to give plasmid pMS43 (Table 2). The choice of *gspO* was motivated by its position
173 downstream of the Sxy-activated gene *gspM* in the chitinase T2SS operon in *E. coli* K-12
174 (Sinha *et al.*, 2009), suggesting a functional link of this secretion system with T4PS. The only
175 other T4aP-related chromosomal gene *yggR* encoding the putative retraction ATPase, was
176 not included in our construct, with the aim to reconstitute efficient T4aP assembly,
177 independent on putative retraction.

178 The pMS10 and pMS43 constructs were introduced in *E. coli* PAP7460 strain to
179 examine production of and assembly of PpdD. In bacteria grown of LB, the expression of
180 *ppdD*, the first gene in the artificial operon, from plasmid pMS10 was almost indistinguishable
181 from the negative control containing vector alone, as revealed with anti-PpdD antibodies (Fig.
182 3A, lanes 1 and 3). A faint band corresponding to mature (GspO-processed) PpdD was
183 detected in the strain with plasmid pMS43 (Fig. 3A, lane 2). To test whether Sxy would
184 activate expression of the artificial *ppd-hof* operon, we cloned the *E. coli* *sxy* gene with its
185 197-bp upstream region under control of the *placZ* promoter on plasmid pCHAP8746 (Table
186 2). Co-expression of *sxy* in strain PAP7460 in the presence of isopropyl β -D-1-
187 thiogalactopyranoside (IPTG) induced both plasmid- and chromosome-encoded PpdD
188 production (Fig. 3A, 4-6). Partial PpdD processing was observed in the presence of pMS10
189 and vector, showing limiting activity of *E. coli* prepilin peptidases. The increase of PpdD
190 levels required Sxy auto-regulation and was only observed with constructs containing the
191 CRP-S site upstream of the *sxy* gene (Fig. S2), confirming previous findings (Jaskolska &
192 Gerdes, 2015). We next tested pilus assembly on bacteria grown on LB or minimal glycerol
193 plates. Pili were sheared from the bacterial surface as described (Luna Rico *et al.*, 2018)
194 (Experimental procedures), followed by analysis of cell and sheared fractions by
195 immunodetection with anti-PpdD antibodies. Only a low amount of PpdD pili was found in the
196 sheared fraction of bacteria producing mature PpdD from plasmid pMS43 cultured on
197 minimal medium (Fig. 3B), suggesting that factors or conditions inducing pilus assembly
198 might be missing. We hypothesized that the DNA flanking the T4aPS-coding genes might

199 have caused inefficient translation of one or more components of the system or, alternatively,
200 that Sxy overexpression might have activated the chromosomal retraction ATPase gene
201 *yggR* to reduce piliation.

202

203 *Optimization of the construct, bacterial hosts and culture conditions*

204

205 To improve piliation efficiency and to render the expression of T4PS genes independent on
206 Sxy, we sequentially eliminated noncoding DNA from individual *ppd/hof* gene clusters in the
207 artificial operon, taking advantage of unique restriction sites that we had introduced in the
208 pMS10 and pMS43 constructs (Experimental procedures). We further placed the resulting
209 operon under control of inducible promoters, *placZ* in plasmid pMS39 or *ppuIC* (a maltose-
210 inducible promoter controlling expression of the *Klebsiella* T2SS *pul* gene cluster) in pMS40.

211 These plasmids were introduced in strain PAP7460 and bacteria were cultured on LB
212 selective plates with or without inducers, as indicated. Piliation assays showed improved
213 *ppdD* expression, in the absence of Sxy. Compared to the pMS43 plasmid, *ppdD* expression
214 was improved in both "next generation" constructs. However, while inducible piliation was
215 observed in strains carrying pMS39 (Fig. 3C), the pMS40 construct did not promote efficient
216 pilus assembly, even when PpdD levels were induced by maltose (Fig. 3C lane 8). Further
217 improvement of piliation efficiency for plasmid pMS39 was achieved by varying the *E. coli*
218 expression hosts (Fig. 3D), and by culture on minimal media supplemented with 0.5 %
219 glycerol (Fig. 3D, lanes 6, 7). For further assays, we chose the parental strain of the Keio
220 gene knockout collection, BW25113 (Baba *et al.*, 2006) and bacterial culture for 72 hours on
221 M9 glycerol plates containing the IPTG at 30°C. Linear map of the *ppd-hof* artificial operon
222 on plasmid pMS39 is shown in Fig. 3E.

223 To probe the specificity and requirements for pilus assembly, we tested the effects of
224 several gene deletions in plasmid pMS39. As expected, no PpdD was detected in strains
225 with plasmid pMS41 (Table 2) lacking the major pilin gene *ppdD* (Fig. 3F). Complementation
226 with *ppdD* cloned on a compatible plasmid pCHAP8565 restored piliation, although

227 overproduction of PpdD led to accumulation of its unprocessed form. Deletions of the gene
228 encoding the polytopic IM platform protein (Δ hofC) and of the minor pilin operon *ppdAB-*
229 *ygdB-ppdC* (Δ MP) also abolished pilus assembly, and piliation was restored upon expression
230 of the corresponding genes *in trans* (Fig. 3F).

231

232 *Observation of pili by immunofluorescence microscopy*

233

234 Previous studies showed that PpdD pili could be assembled by the related heterologous
235 machinery, the *K. oxytoca* pullulanase T2SS (Sauvonnet *et al.*, 2000b, Cisneros *et al.*,
236 2012b). To compare PpdD pilus assembly in the heterologous T2SS and in the reconstituted
237 T4P system, we transformed strain BW25113 F' *lacI*^Q with pMS41 (encoding the T4aPS
238 Δ *ppdD*) or pCHAP8184 (encoding the T2SS lacking the major pseudopilin PulG) (Table 2).
239 We complemented these strains with *ppdD* cloned on plasmid pCHAP8565 and probed for
240 conditions that would allow comparable pilus assembly in both systems in bacteria cultured
241 on minimal glycerol plates. As shown in Fig. 4A, lanes 1 and 2, pili were assembled in both
242 strains in the absence of induction. Maltose, the inducer of T2SS gene expression, lowered
243 PpdD levels and pilus assembly efficiency (Fig. 4A, lanes 5, 6). Induction of the *hof-ppd*
244 operon and *ppdD* by IPTG allowed for more efficient piliation in both systems (Fig. 4A, lanes
245 3 and 4).

246 The possibility to use different Tff assembly systems for PpdD polymerization provides a
247 unique opportunity to study the relative influence of pilin subunits and the assembly
248 machinery on fibre structure and properties. We used immunofluorescence microscopy to
249 compare pilus assembly *via* the two systems in bacteria cultured in M9 glycerol plates in the
250 presence of IPTG (Fig. 4A, lanes 3,4). Similar numbers of PpdD pili were assembled by the
251 T2SS (top panels, B-E) and T4PS (bottom panels, F-I). Both fibres appeared highly similar in
252 terms of length and apparent thickness, although PpdD pili assembled by the heterologous
253 T2SS appeared somewhat more curved and flexible. We noted that T4PS- assembled pili

254 were more often attached to the bacterial cells when compared to those assembled by the
255 T2SS.

256

257 *Analysis of PpdD pili by electron microscopy*

258

259 To better compare how the two systems, T2SS and T4PS, affect the PpdD pilus assembly,
260 we imaged the two types of PpdD pili by using both negative stain electron microscopy (EM)
261 and cryo-EM. The analysis of negatively stained pili by EM showed somewhat higher
262 conformational heterogeneity and flexibility for the T2SS-assembled pili (Fig. 5), consistent
263 with the IF results.

264 We determined the helical symmetry of the pili assembled by the two different
265 systems based on the averaged power spectra of segments imaged by cryo-EM (Fig.6C&D).
266 Within both of the two averaged power spectra we found dominant layer lines at $1/(14.7\text{\AA})$,
267 $1/(20.3\text{\AA})$, $1/(53.2\text{\AA})$ and $1/(159.5\text{\AA})$, indicating that they have an indistinguishable helical
268 symmetry. Each subunit is related to an adjacent subunit by, on average, a $\sim 11.2\text{\AA}$ axial rise
269 and $\sim 96.0^\circ$ azimuthal rotation, forming a 1-start right-handed helix, although these
270 parameters are quite variable in PpdD. This symmetry is very typical for Type IV pili, such as
271 those from *P. aeruginosa* (Wang *et al.*, 2017), *N. gonorrhoeae* (Wang *et al.*, 2017) and *N.*
272 *meningitidis* (Kolappan *et al.*, 2016) (Table 3). The symmetry of PpdD pili differs from that of
273 PulG pseudopili assembled by the same T2SS, which showed $\sim 10.2\text{\AA}$ axial rise and 83.2° of
274 twist (Lopez-Castilla *et al.*, 2017). The difference between pseudopilus and pilus helical
275 parameters, as well as the similarity of these parameters between PpdD pili assembled by
276 the two systems suggest that the PpdD subunit itself, and not the assembly machinery, is the
277 main determinant of subunit packing and fibre structure.

278

279 *Pilin interactions with T4P assembly components*

280

281 To examine how PpdD interacts with its cognate assembly apparatus, we employed the
282 bacterial two-hybrid approach (BAC2H) (Karimova *et al.*, 1998), used previously to study
283 interactions of T4P assembly components in *P. aeruginosa* (Nguyen *et al.*, 2015) and *N.*
284 *meningitidis* (Georgiadou *et al.*, 2012). The *ppd* and *hof* genes encoding full-length mature
285 proteins were fused to genes encoding T18 and T25 fragments of the *Bordetella pertussis*
286 CyaA toxin catalytic domain (Experimental procedures). We co-transformed the *E. coli cya*
287 deletion strain DHT1 with selected plasmids and measured the reconstitution of adenylyl
288 cyclase activity and induction of the chromosomal *lacZ* gene, dependent on interactions
289 between the hybrid proteins. As shown in Fig. 7A, PpdD formed homo-dimers in this assay
290 and interacted with the IM assembly components HofN and HofO. In addition, we detected
291 homo-dimerization of HofB ATPase, whereas HofN and HofO formed heterodimers, as
292 shown previously in T4P systems of *N. meningitidis* (Georgiadou *et al.*, 2012) and *P.*
293 *aeruginosa* (Leighton *et al.*, 2015b). PpdD also interacted specifically with the minor pilin
294 PpdB.

295 Assembly of PpdD T4 pilin by the heterologous T2SS suggests its productive
296 interactions with one or several components of the PulG pseudopilus assembly system in the
297 inner membrane. To identify these contacts, we compared interactions of PpdD with T2SS
298 components to those of PulG, the cognate major pseudopilin of this system characterized
299 previously (Nivaskumar *et al.*, 2016). T18-PulG and T18-PpdD chimera were tested with
300 several T25-Pul T2SS component hybrids (Experimental procedures) (Figs. 7C and D). As
301 shown previously, the major pseudopilin PulG forms dimers in the membrane and interacts
302 with PulM and PulF components of the assembly platform, as well as with the minor
303 pseudopilins PulH and PulJ (Nivaskumar *et al.*, 2016). PpdD showed interaction signals with
304 PulF and PulH similar to those of PulG (Fig. 7D). Like PulG, PpdD did not interact with PulC
305 or PulL IM AP components. In contrast to PulG, PpdD did not interact with the minor
306 pseudopilin PulJ, which is part of the minor pseudopilin initiation complex in the T2SS
307 (Korotkov & Hol, 2008, Cisneros *et al.*, 2012a). PpdD interaction with PulM, the AP
308 component involved in pseudopilin targeting to the assembly machinery (Nivaskumar *et al.*,

309 2016, Santos-Moreno *et al.*, 2017) was significantly weaker than that of PulG (Fig. 7D). Since
310 the N-terminal domains of PulG and PpdD are highly conserved, this is likely due to
311 differences between the periplasmic domains of these major Tff subunits.

312

313

314 **Discussion**

315

316 We report here the functional reconstitution of a 13-component trans-envelope complex
317 involved in T4aP assembly in *E. coli*. Previously, similar reconstitutions have been achieved
318 for pili of the T4b subclass encoded by single gene clusters (Sohel *et al.*, 1996, Stone *et al.*,
319 1996, Yuen *et al.*, 2013). The reconstitution of the complete T4aP system from several
320 operons, although somewhat more challenging, was greatly facilitated by the Gibson
321 assembly approach, which allows assembly of multiple DNA fragments in a single step
322 (Gibson *et al.*, 2009). In the case of the *ppd-hof* operon, the successful cloning strategy
323 consisted of minimizing the presence of noncoding regions, which may affect gene
324 expression at post-transcriptional level. A similar approach may be used to reconstitute
325 diverse nanomachines from model bacteria that are highly pathogenic or toxinogenic, non-
326 cultivable or recalcitrant to genetic manipulation.

327

328 The reconstituted EHEC T4PS contains 13 components. Of note, the artificial *ppd-hof*
329 operon does not encode an equivalent of a pilotin like PilF in *P. aeruginosa* (Koo *et al.*, 2013)
330 or PilW in *Neisseria* (Szeto *et al.*, 2011) required for the correct targeting and assembly of
331 the secretin in the OM. Although PilF homologue is absent in the *E. coli* genome, we cannot
332 exclude that another *E. coli* OM lipoprotein or the Bam machinery itself support PilQ
333 assembly. We show that, in addition to PpdD and a prepilin peptidase, HofC and four minor
334 pilins together are essential for pilus assembly on the bacterial surface. The essential role of
335 HofC homologue in *P. aeruginosa* PilC (Takhar *et al.*, 2013) has been recently confirmed for
336 *N. meningitidis* PilG (Goosens *et al.*, 2017). In the latter study, a synthetic approach was

337 employed to assemble meningococcal T4P in the periplasm of *E. coli* and only 8 proteins
338 were essential. Besides the HofC equivalent PilG, these included the major pilin, prepilin
339 peptidase, the HofB equivalent PilF and PilM, PilN, PilO and PilP assembly components.
340 PilQ and PilW, which allow for pilus surface presentation, were not required for pilus
341 assembly *per se*, but neither were the minor pilins (Goosens *et al.*, 2017). This is in contrast
342 to our results and to those showing that minor pilins in *P. aeruginosa* promote pilus assembly
343 initiation (Nguyen *et al.*, 2015). Although minor pseudopilins are not fully essential for
344 pseudopilus assembly, they greatly improve its efficiency (Cisneros *et al.*, 2012a). CryoEM
345 tomography studies of *Myxococcus* T4PS suggests that pilins stabilize the AP complex
346 (Chang *et al.*, 2016). The fact that minor pilins are dispensable for pilus assembly in the
347 reconstituted meningococcal T4PS could be explained therefore by the high-level expression
348 of genes encoding PilE and assembly components controlled by the T7 promoter (Goosens
349 *et al.*, 2017). Nevertheless, minor pilins are essential for function in T4P and T2SS (Helaine
350 *et al.*, 2005, Giltner *et al.*, 2010, Sauvonnet *et al.*, 2000b, Cisneros *et al.*, 2012b, Cehovin *et*
351 *al.*, 2013) and their binding to specific substrates has been shown in several systems
352 (Cehovin *et al.*, 2013, Douzi *et al.*, 2011). Recent studies of *Vibrio* T4aP involved in
353 competence strongly suggest that minor pilins mediate DNA binding *via* the pilus tip (Ellison
354 *et al.*, 2018).

355

356 Reconstitution of *E. coli* T4aPS allowed us to compare the symmetry of fibres
357 produced by the cognate assembly machinery with those assembled by the T2SS.
358 Regardless of the system that promoted their polymerization, PpdD pili showed dominant
359 azimuthal rotation of 96° and axial rise of 11.2 Å. Minor pseudopilins priming assembly of
360 PpdD fibres in the T2SS, or minor pilins priming assembly in the cognate T4PS had no
361 influence on this symmetry. Conversely, assembly of the cognate substrate PulG of the *K.*
362 *oxytoca* T2SS resulted in different fibres with the twist of 83.2° and rise of 10.2 Å (Lopez-
363 Castilla *et al.*, 2017). Together, these results show that major (pseudo)pilin subunits, through
364 their specific packing and interfaces, determine the overall symmetry parameters.

365

366 Although *K. oxytoca* T2SS promotes assembly of PpdD, it does not assemble other
367 major pilins including *P. aeruginosa* PilA or the gonococcal PilE (Kohler *et al.*, 2004),
368 suggesting selective substrate recognition in Tff nanomachines. Although non-exhaustive,
369 our BAC2H results provide insights into the basis of this heterologous assembly. In T2SS,
370 PpdD interacts strongly with PulH, which shares 19% identity with its cognate minor pilin
371 PpdB (Fig. S3A), perhaps explaining why the *Klebsiella* T2SS and *E. coli* T4aPS minor
372 (pseudo)pilins are partially interchangeable (Cisneros *et al.*, 2012b). Strong sequence
373 conservation of PulG and PpdD N-terminal segments (Fig. S3B) is consistent with their
374 similar interactions with PulF and shared ability to interact with PulM. Indeed, important
375 determinants of PulM interaction were mapped to the N-terminal region of PulG (Nivaskumar
376 *et al.*, 2016, Santos-Moreno *et al.*, 2017). However, PulM interaction with PpdD was
377 significantly weaker than that with PulG, suggesting that globular domains of these proteins
378 are also involved. In support of this idea, periplasmic domain of *Thermus thermophilus* PilA
379 binds to PilM-PilN complex *in vitro* (Karuppiyah *et al.*, 2013). Two AP components of the
380 EHEC system, HofN and HofO, are the main interacting partners of PpdD and share the
381 same topology with PulM. Like PulM, with which it shares 25% identity (Fig. S3C), HofN is
382 highly positively charged (pKi >10), whereas PulG and PpdD are acidic (pKi of 4.4 and 4.7,
383 respectively). Further biochemical and structural analyses will be required to understand the
384 molecular basis of pilin selectivity, likely crucial for assembly.

385

386 Upon induction of the *ppd-hof* expression on plasmid pMS39 about 50% of PpdD was
387 assembled into pili, which is comparable to the efficiency observed for other T4PSs
388 expressed from the host chromosomes (Giltner *et al.*, 2010). Bypassing the need for Sxy and
389 excluding the *yggR* gene from the artificial operon allowed us to reconstitute pilus assembly,
390 dissociated from retraction. Since competence pili appear to be less abundant compared to
391 T4P involved in motility and adherence (Ellison *et al.*, 2018), this strategy facilitated pilus
392 purification for ultrastructural studies. However, to assess the function of EHEC T4aP in DNA

393 uptake or twitching motility, future studies should include the antagonistic YggR ATPase to
394 reconstitute a fully functional and dynamic system. Studies in *V. cholerae* demonstrated the
395 long-proposed role of pilus retraction in DNA uptake (Seitz & Blokesch, 2013), but also
396 showed that low levels of retraction and transformation can be observed in *pilT* mutants
397 (Ellison *et al.*, 2018).

398 In *V. cholerae*, T4PS is induced by chitin oligosaccharides (Meibom *et al.*, 2005),
399 which activate transcription of a small RNA that stimulates *sxy* translation (Yamamoto *et al.*,
400 2011). Although there is no evidence for a similar translational regulation of *sxy* in *E. coli*
401 (Jaskolska & Gerdes, 2015), specific starvation or other signals appear to induce *sxy*
402 expression and its regulon in EHEC strains leading to pilus assembly (Xicohtencatl-Cortes *et*
403 *al.*, 2007). The *hofMNOPQ* operon is required for growth on extracellular DNA as carbon
404 source, which might also act as an inducer (Palchevskiy & Finkel, 2006). In addition, Sxy-
405 and HofQ-dependent DNA uptake has been observed in *E. coli* K-12 (Sinha & Redfield,
406 2012). T4PS might be involved in DNA repair and horizontal gene transfer in mixed bacterial
407 populations and biofilms, where extracellular DNA is abundant (Ibáñez de Aldecoa *et al.*,
408 2017). Recently, by using time-lapse fluorescence imaging, DNA uptake mediated by the
409 Sxy-controlled T4aP has been observed in *Vibrio* and mutational analysis implicated minor
410 pilins in DNA binding to the pilus tip (Ellison *et al.*, 2018). Whether T4aP from *E. coli* and
411 related species also mediate DNA binding, uptake and exchange is a fascinating question
412 that deserves further study (Veening & Blokesch, 2017). Although the genes encoding T4aP
413 are present and conserved in all enterobacteria, their biological role and conditions that
414 induce their expression are poorly understood. Reconstitution of a complex multi-component
415 pilus assembly system from an enterobacterial class III pathogen in a non-pathogenic *E. coli*
416 strain should facilitate future studies of its biological function and assembly mechanism.

417

418 **Experimental procedures**

419

420 *Bacterial strains and culture conditions*

421

422 The *E. coli* strains used in this study are listed in Table 1. Bacteria were grown at 30°C in LB
423 or minimal M9 medium containing 0.5% glycerol as the carbon source (Miller, 1972). Media
424 were supplemented with 0.5 mM IPTG or 0.2 % D-maltose. Antibiotics were added at
425 following concentrations: ampicillin (Ap), 100 µg.mL⁻¹, chloramphenicol (Cm), 25 µg.mL⁻¹,
426 kanamycin (Km), 25 µg.mL⁻¹ and zeocin (Ze), 8 µg.mL⁻¹. An indicator of β-galactosidase
427 activity 5-bromo-4-chloro-3-indolyl-β-D-galactopyranoside (X-gal) was added to LB media at
428 40 µg.mL⁻¹.

429

430 *Plasmid constructions*

431

432 The list of plasmids used in this study is given in Table 2. To build the synthetic operon the
433 three gene clusters were PCR amplified from the chromosomal DNA of strain EDL933,
434 together with ~100-bp flanking non-coding sequences using primers (1 to 6) listed in
435 Supplemental Table S1. A fragment of pBR322 vector containing Ap^R and *ori* region was
436 PCR-amplified with primers 7 and 8 (Table S1). The primers were designed to generate
437 fragments with 20-bp overlap, following the Gibson assembly manual (New England
438 Biolabs). Following *DpnI* digestion of the PCR fragments generated with Phusion enzyme,
439 the 4-fragment Gibson assembly reaction was performed as suggested by the manufacturer.
440 The reaction mix was transformed into ultracompetent bacteria of strain DH5α. The resulting
441 plasmid pMS10 was purified and fully sequenced (GATC).

442

443 Plasmid pMS37 was obtained by successively replacing each gene cluster with a
444 corresponding fragment lacking the noncoding DNA, leaving only the Shine-Dalgarno regions
445 of the first gene in each operon. These minimal operon fragments were PCR-amplified from
446 the EDL933 DNA using primers 9 – 14 (Table S1) and digested with *DpnI*. Fragments were
447 individually replaced by directed cloning, by ligating the new PCR fragments with the electro-
eluted vector sequences digested with the same enzymes: *AflIII-NcoI* for fragment *ppdD*-

448 *hofBC*, NcoI-Ascl for fragment *hofMNOPQ*, and Ascl-NotI restriction sites for fragment
449 *ppdAB-ygdB-ppdC* to yield plasmid pMS37. Plasmid pMS37 was digested with NotI and XhoI
450 to introduce the *gspO* gene, PCR amplified from the MG1655 DNA using primers 15 and 16
451 to give pMS38. Addition of the *lacZ* promoter (PCR amplified from pSU18 vector using
452 primers 17, 18) into pMS38 using EcoRI-Clal sites produced the plasmid pMS39.
453 Introduction of the *puIC* promoter (PCR-amplified from plasmid pCHAP8185 using primers
454 19, 20) into pMS38 using the same restriction sites produced the plasmid pMS40. Plasmid
455 pMS43 was obtained by cloning the 1623-bp BsiWI-NotI fragment from plasmid pMS39 into
456 pMS10 digested with the same enzymes.

457 To generate plasmid pMS41, the *hofB-hofC* fragment, PCR-amplified with primers hofB AfIII
458 5 and hofC N NcoI 3, was cloned into pMS39 digested with AfIII and NcoI. Plasmid pMS47
459 was generated by cloning the *ppdD-hofB* fragment with primers ppdD AfI 5 and HofB Nco 3
460 into the pMS39 AfIII-NcoI A fragment of 9507 bp. To generate plasmid pMS45 plasmid
461 pMS39 was digested with Ascl and NotI and the resulting 10028-bp fragment was treated
462 with T4 polymerase before being religated.

463 For the bacterial two-hybrid constructs, *ppd* and *hof* genes were fused in frame to the C-
464 terminal end of *cyaA* fragments in plasmids pUT18c and pKT25 by cloning PCR-amplified
465 *ppd/hof* genes flanked by Kpn and EcoRI sites. For pilin genes, only the sequences encoding
466 mature (prepilin peptidase processed) protein regions were included. The list of primers
467 (Eurofins) used for these constructs is given in Table S1. All clones were verified by
468 sequencing (GATC and Eurofins).

469

470 *Pilus assembly assay*

471

472 Pilus assembly assays were performed as described previously (Campos *et al.*, 2010) (Luna
473 Rico *et al.*, 2018). Briefly, *E. coli* strains containing indicated plasmids were grown at 30°C
474 for 48-72 hr on LB or M9 agar supplemented as required with inducers and antibiotics.
475 Bacteria were scraped off the plates and resuspended in LB and normalized to 1 OD₆₀₀ ml⁻¹.

476 Suspensions were vortexed for 1 min to detach surface pili and centrifuged at ~12000 x g for
477 5 minutes at 4°C. The pelleted bacteria were resuspended in SDS sample buffer at 10 OD₆₀₀
478 mL⁻¹. The supernatants were spun at ~12000 x g for another 10 minutes and 0.7 ml was
479 transferred to a clean tube and submitted to precipitation with 10 % trichloroacetic acid. After
480 incubation for 30 minutes on ice and centrifugation at ~12000 x g for 30 minutes at 4°C, the
481 pellets were washed twice with cold acetone, air-dried and resuspended in SDS sample
482 buffer. Equivalent amounts of cell and sheared fractions were analysed by denaturing
483 polyacrylamide gel electrophoresis (PAGE) on 10% slab gels using the Tris-Tricin separation
484 system (Schagger & von Jagow, 1987). Proteins were transferred onto nitrocellulose
485 membranes (ECL, Amersham) using the Pierce Power Blotter system (Thermo) and revealed
486 with polyclonal anti-PppD antisera diluted 1:2000, unless otherwise indicated (Sauvonnet *et*
487 *al.*, 2000a). Secondary goat anti-rabbit antibodies coupled to HRP (GE) were diluted to 1:20
488 000. Blots were revealed by ECL2 (Thermo) and fluorescence signal was recorded on
489 Typhoon FLA9000 phospho-imager (GE). Images were processed with Adobe Photoshop.

490

491 *Immunofluorescence microscopy*

492 Sampled for IF analysis of pili were prepared as described previously (Cisneros *et al.*, 2012b,
493 Luna Rico *et al.*, 2018). Bacteria were grown for 48 hours at 30°C on LB agar supplemented
494 with antibiotics and inducer (0.4% maltose or 0.5 mM IPTG, as indicated) were carefully
495 resuspended in PBS at 1 OD₆₀₀.ml⁻¹ and immobilized on coverslips coated with poly-L-lysine.
496 After 30 minutes of fixation using 3.7% formaldehyde at room temperature, reactions were
497 quenched with 1M Tris-HCl pH 8.0 and samples were blocked with 1% bovine serum
498 albumin (BSA) in PBS. Pili were detected using an anti-PpdD antibody (1:1000) and a
499 secondary anti-rabbit IgG coupled to Alexa Fluor 488 (1:200); bacteria were stained with 4',6-
500 diamidino-2-phenylindole (DAPI). Samples were observed with an Axio Imager A2
501 microscope (Zeiss) and images were acquired with the AxioCam MRm digital camera
502 connected to the microscope. Images were analysed with Zen 2012 software (Zeiss) and
503 processed with Adobe Photoshop.

504

505 *Preparation of pili*

506

507 Ten 90-mm LB plates containing Ap, Cm and IPTG were inoculated with BW25113 F'*lacI*⁰
508 strain containing plasmid pCHAP8565 and either pCHAP8184 (encoding T2SS) or pMS41
509 (encoding T4PS). Bacteria were cultured for 72 hours at 30°C and harvested in LB medium.
510 Bacterial suspensions were subjected to vortex agitation for 5 min and then passed 10 times
511 through a 21-gauge needle to detach surface pili. Bacteria were removed by centrifugation
512 for 10 min at 10000 g. Supernatants were further centrifuged in Eppendorf tubes for 10 min
513 at 16000xg to pellet the remaining bacteria. Pili from the supernatant fractions were
514 recovered by ultracentrifugation for 1 hour at 100000xg at 4°C. Pili were taken up in 0.1 mL
515 of 50 mM HEPES pH 7.2, 50 mM NaCl and kept on ice before EM analysis.

516

517 *Electron microscopy*

518

519 For the negative stain EM imaging, 3 µl of the PpdD pili sample were applied to previously
520 plasma-cleaned carbon-coated copper grids. After incubating for 30 seconds, the excess
521 sample were removed and stained with 2% uranyl acetate (w / v) before imaging with FEI
522 Tecnai F20 electron microscope at 120 kV. Motioncor2 (Li et al., 2013) was used for motion
523 correcting all the images, following by using CTFFIND3 (Mindell and Grigorieff, 2003) for
524 estimation of the defocus and astigmatism. Filament boxes were selected and extracted by
525 using e2heliboxer within EMAN2 (Tang et al., 2007) on images multiplied by the CTF. The
526 Spider software package (Frank et al., 1996) was used for all further image processing.

527

528

529 *Cryo-EM imaging and helical symmetry comparison*

530

531 PpdD pili sample (3 μ l) assembled from T2SS and T4PS were applied to plasma-cleaned
532 lacey carbon grids. The grids were plunge-frozen in liquid ethane using a Vitrobot Mark IV
533 (FEI). The images were recorded on a Titan Krios microscope at 300kV, using a Falcon III
534 direct electron detector at magnification of 75,000X with a total dose of \sim 45 electrons/ \AA^2 .
535 Motioncor2 was used for motion correcting all the images, following by using CTFFIND3 for
536 estimation of the defocus and astigmatism. Filament boxes were selected and extracted by
537 using e2heliboxer within EMAN2 on images multiplied by the CTF. The Spider software
538 package was used for all further image processing. Segments with a very large out-of-plane
539 tilt as well as with symmetry far from the average were discarded.

540

541 *Bacterial two-hybrid (BAC2H) analysis*

542

543 Competent cells of strain DHT1 (Dautin *et al.*, 2000) were co-transformed with pUT18C and
544 pKT25 plasmid derivatives and bacteria were grown for 48 h at 30°C on LB plates containing
545 Ap and Km. Six colonies were picked at random and inoculated into 5 ml cultures in LB
546 containing Km and Ap, grown overnight and inoculated the next day into fresh medium
547 containing 1 mM IPTG. Bacteria were cultured to mid-log phase and β -galactosidase activity
548 was measured as described (Miller, 1972). At least 2 independent experiments were
549 performed with several randomly picked transformants. Bar graphs represent mean values
550 and error bars indicate standard deviation. The non-parametric Kruskal-Wallis followed by
551 Dunn's multiple comparison tests were used in statistical analysis using the Graphpad Prism
552 7 software.

553

554 **Acknowledgements**

555 This work was funded by the Institut Pasteur, the Centre National de la Recherche
556 Scientifique (CNRS), the French Agence Nationale de la Recherche grant ANR-14-CE09-
557 0004 and NIH grant GM122510 (to E.H.E). We thank Daniel Ladant and members of the
558 BIM, NMR of Biomolecules and Structural Bioinformatics Units in Institut Pasteur for support

559 and helpful discussions. We are grateful to Nadia Izadi-Pruneyre for advice and critical
560 reading of the manuscript. A.L.R. is a fellow of the Pasteur - Paris University (PPU)
561 International PhD program.

562

563 **Author contributions**

564

565 OF and EHE conceived the study and supervised experimental research. ALR, NN, WZ and
566 OF performed experiments. ARL, WZ, OF and EHE analysed the data and wrote the
567 manuscript.

568

569 **Conflict of interest**

570

571 The authors declare that they have no conflict of interest.

572

573

574 **References**

575

- 576 Ayers, M., L.M. Sampaleanu, S. Tammam, J. Koo, H. Harvey, P.L. Howell & L.L. Burrows,
577 (2009) PilM/N/O/P proteins form an inner membrane complex that affects the stability
578 of the *Pseudomonas aeruginosa* type IV pilus secretin. *J. Mol. Biol.* **394**: 128-142.
- 579 Baba, T., T. Ara, M. Hasegawa, Y. Takai, Y. Okumura, M. Baba, K.A. Datsenko, M. Tomita,
580 B.L. Wanner & H. Mori, (2006) Construction of *Escherichia coli* K-12 in-frame, single-
581 gene knockout mutants: The Keio collection. *Mol Syst Biol* **2**: 2006.0008.
- 582 Bartolome, B., Y. Jubete, E. Martinez & F. de la Cruz, (1991) Construction and properties of
583 a family of pACYC184-derived cloning vectors compatible with pBR322 and its
584 derivatives. *Gene* **102**: 75-78.
- 585 Berry, J.L. & V. Pelicic, (2015) Exceptionally widespread nanomachines composed of type IV
586 pilins: the prokaryotic Swiss Army knives. *FEMS Microbiol Rev* **39**: 134-154.
- 587 Berry, J.L., Y. Xu, P.N. Ward, S.M. Lea, S.J. Matthews & V. Pelicic, (2016) A comparative
588 structure/function analysis of two type IV pili DNA receptors defines a novel mode of
589 DNA binding. *Structure.* **24**: 926-934.
- 590 Bolivar, F., R.L. Rodriguez, P.J. Greene, M.C. Betlach, H.L. Heyneker, H.W. Boyer, J.H.
591 Crosa & S. Falkow, (1977) Construction and characterization of new cloning vehicles.
592 II. A multipurpose cloning system. *Gene* **2**: 95-113.
- 593 Cameron, A.D.S. & R.J. Redfield, (2006) Non-canonical CRP sites control competence
594 regulons in *Escherichia coli* and many other gamma-proteobacteria. *Nucl. Acids Res.*
595 **34**: 6001-6014.
- 596 Campos, M., M. Nilges, D.A. Cisneros & O. Francetic, (2010) Detailed structural and
597 assembly model of the type II secretion pilus from sparse data. *Proc Natl Acad Sci*
598 *USA* **107**: 13081–13086.

599 Cehovin, A., P.J. Simpson, M.A. McDowell, D.R. Brown, R. Noschese, M. Pallett, J. Brady,
600 G.S. Baldwin, S.M. Lea, S.J. Matthews & V. Pelicic, (2013) Specific DNA recognition
601 mediated by a type IV pilin. *Proc Natl Acad Sci USA* **110**: 3065-3070.

602 Chang, Y.W., L.A. Rettberg, A. Treuner-Lange, J. Iwasa, L. Sogaard-Andersen & G.J.
603 Jensen, (2016) Architecture of the type IVa pilus machine. *Science* **351**: aad2001.

604 Cisneros, D.A., P.J. Bond, A.P. Pugsley, M. Campos & O. Francetic, (2012a) Minor
605 pseudopilin self-assembly primes type II secretion pseudopilus elongation. *EMBO J*
606 **31**: 1041-1053.

607 Cisneros, D.A., G. Pehau-Arnaudet & O. Francetic, (2012b) Heterologous assembly of type
608 IV pili by a type II secretion system reveals the role of minor pilins in assembly
609 initiation. *Mol Microbiol* **86**: 805-818.

610 Craig, L., R.K. Taylor, M.E. Pique, B.D. Adair, A.S. Arvai, M. Singh, S.J. Lloyd, D.S. Shin,
611 E.D. Getzoff, M. Yeager, K.T. Forest & J.A. Tainer, (2003) Type IV pilin structure and
612 assembly: X-ray and EM analyses of *Vibrio cholerae* toxin-coregulated pilus and
613 *Pseudomonas aeruginosa* PAK pilin. *Mol Cell* **11**: 1139-1150.

614 Datsenko, K.A. & B.L. Wanner, (2000) One-step inactivation of chromosomal genes in
615 *Escherichia coli* K-12 using PCR products. *Proc Natl Acad Sci USA* **97**: 6640–6645.

616 Dautin, N., G. Karimova, A. Ullmann & D. Ladant, (2000) Sensitive genetic screen for
617 protease activity based on a cyclic AMP signaling cascade in *Escherichia coli*. *J*
618 *Bacteriol* **182**: 7060-7066.

619 de Amorim, G.C., D.A. Cisneros, M. Delepierre, O. Francetic & N. Izadi-Pruneyre, (2014) 1H,
620 15N and 13C resonance assignments of PpdD, a type IV pilin from
621 enterohemorrhagic *Escherichia coli*. *Biomol NMR Assign*. **8**: 43-46.

622 Douzi, B., G. Ball, C. Cambillau, M. Tegoni & R. Voulhoux, (2011) Deciphering the Xcp
623 *Pseudomonas aeruginosa* type II secretion machinery through multiple interactions
624 with substrates. *J Biol Chem* **286**: 40792-40801.

625 Ellison, C.K., T.N. Dalia, A.V. Ceballos, J.C. Wang, N. Biais, Y.V. Brun & A.B. Dalia, (2018)
626 Retraction of DNA-bound type IV competence pili initiates DNA uptake during natural
627 transformation in *Vibrio cholerae*. *Nat Microbiol* **3**: 773-780.

628 Ellison, C.K., J. Kan, R.S. Dillard, D.T. Kysela, A. Ducret, C. Berne, C.M. Hampton, Z. Ke,
629 E.R. Wright, N. Biais, A.B. Dalia & Y.V. Brun, (2017) Obstruction of pilus retraction
630 stimulates bacterial surface sensing. *Science* **368**: 535-538.

631 Francetic, O., D. Belin, C. Badaut & A.P. Pugsley, (2000) Expression of the endogenous type
632 II secretion pathway in *Escherichia coli* leads to chitinase secretion. *The EMBO J* **19**:
633 6697-6703.

634 Francetic, O., S. Lory & A.P. Pugsley, (1998) A second prepilin peptidase gene in
635 *Escherichia coli* K-12. *Mol Microbiol* **27**: 763-775.

636 Frank, J., Radermacher, M., Penczek, P., Zhu, J., Li, Y., Ladjadj, M., and Leith, A. (1996).
637 SPIDER and WEB: Processing and visualization of images in 3D electron microscopy
638 and related fields. *J. Struct Biol* **116**: 190-199.

639 Fullner, K.J. & J.J. Mekalanos, (1999) Genetic characterization of a new type IV-A pilus gene
640 cluster found in both classical and El Tor biotypes of *Vibrio cholerae*. *Infect. Immun.*
641 **67**: 1393–1404.

642 Georgiadou, M., M. Castagnini, G. Karimova, D. Ladant & V. Pelicic, (2012) Large-scale
643 study of the interactions between proteins involved in type IV pilus biology in
644 *Neisseria meningitidis*: characterization of a subcomplex involved in pilus assembly.
645 *Mol Microbiol* **84**: 857-873.

646 Gibson, D.G., L. Young, R.Y. Chuang, J.C. Venter, C.A. Hutchison, 3rd & H.O. Smith, (2009)
647 Enzymatic assembly of DNA molecules up to several hundred kilobases. *Nat.*
648 *Methods* **6**: 343–345.

649 Giltner, C.L., M. Habash & L.L. Burrows, (2010) *Pseudomonas aeruginosa* minor pilins are
650 incorporated into Type IV Pili. *J Mol Biol* **398**: 444-461.

651 Gold, V.A., R. Salzer, B. Averhoff & W. Kuhlbrandt, (2015) Structure of a type IV pilus
652 machinery in the open and closed state. *Elife* **4**. doi: 10.7554/eLife.07380.

653 Goosens, V.J., A. Busch, M. Georgiadou, M. Castagnini, K.T. Forest, G. Waksman & V.
654 Pelicic, (2017) Reconstitution of a minimal machinery capable of assembling
655 periplasmic type IV pili. *Proc Natl Acad Sci USA* **114**: E4978-E4986.

656 Helaine, S., E. Carbonelle, L. Prouvensier, J.-L. Beretti, X. Nassif & V. Pelicic, (2005) PilX, a
657 pilus-associated protein essential for bacterial aggregation, is a key to pilus-facilitated
658 attachment of *Neisseria meningitidis* to human cells. *Mol Microbiol* **55**: 65-77.

659 Helaine, S., D.H. Dyer, X. Nassif, V. Pelicic & K.T. Forest, (2007) 3D structure/function
660 analysis of PilX reveals how minor pilins can modulate the virulence properties of
661 type IV pili. *Proc Natl Acad Sci USA* **104**: 15888-15893.

662 Hospenthal, M., T.R.D. Costa & G. Waksman, (2017) A comprehensive guide to pilus
663 biogenesis in Gram-negative bacteria. *Nat Rev Microbiol* **15**: 365-379.

664 Ibáñez de Aldecoa, A.L., O. Zafra & J.E. González-Pastor, (2017) Mechanisms and
665 regulation of extracellular DNA release and its biological roles in microbial
666 communities. *Frontiers Microbiol* **8**: 1390.

667 Jaskolska, M. & K. Gerdes, (2015) CRP-dependent positive autoregulation and proteolytic
668 degradation regulate competence activator Sxy of *Escherichia coli*. *Mol Microbiol* **95**:
669 833-845.

670 Karimova, G., J. Pidoux, A. Ullmann & D. Ladant, (1998) A bacterial two-hybrid system
671 based on a reconstituted signal transduction pathway. *Proc Natl Acad Sci USA* **95**:
672 5752-5756.

673 Karuppiah, V., R.F. Collins, A. Thistlethwaite, Y. Gao & J.P. Derrick, (2013) Structure and
674 assembly of an inner membrane platform for initiation of type IV pilus biogenesis.
675 *Proc Natl Acad Sci USA* **110**: E4638-4647.

676 Kohler, R., K. Schafer, S. Muller, G. Vignon, K. Diederichs, A. Philippsen, P. Ringler, A.P.
677 Pugsley, A. Engel & W. Welte, (2004) Structure and assembly of the pseudopilin
678 PulG. *Mol Microbiol* **54**: 647-664.

679 Kolappan, S., M. Coureuil, X. Yu, X. Nassif, E.H. Egelman & L. Craig, (2016) Structure of the
680 *Neisseria meningitidis* Type IV pilus. *Nat Commun* **7**: 13015.

681 Koo, J., R.P. Lamers, J.L. Rubinstein, L.L. Burrows & L.P. Howell, (2016) Structure of the
682 *Pseudomonas aeruginosa* type IVa pilus secretin at 7.4 Å. *Structure* **24**: 1778-1787.

683 Koo, J., T. Tang, H. Harvey, S. Tammam, L.M. Sampaleanu, L.L. Burrows & L.P. Howell,
684 (2013) Functional mapping of PilF and PilQ in the *Pseudomonas aeruginosa* type IV
685 pilus system. *Biochemistry* **52**: 2914-2923.

686 Korotkov, K.V. & W.G. Hol, (2008) Structure of the GspK-GspI-GspJ complex from the
687 enterotoxigenic *Escherichia coli* type 2 secretion system. *Nat Struct Mol Biol* **15**: 462-
688 468.

689 Ledesma, M.A., S.A. Ochoa, A. Cruz, L.M. Rocha-Ramírez, J. Mas-Oliva, C.A. Eslava, J.A.
690 Girón & J. Xicohtencatl-Cortes, (2010) The Hemorrhagic Coli Pilus (HCP) of
691 *Escherichia coli* O157:H7 is an inducer of proinflammatory cytokine secretion in
692 intestinal epithelial cells. *PLoS One* **5**: e12127.

693 Leighton, T.L., R.N. Buensuceso, P.L. Howell & L.L. Burrows, (2015a) Biogenesis of
694 *Pseudomonas aeruginosa* type IV pili and regulation of their function. *Environ*
695 *Microbiol* **17**: 4148-4163.

696 Leighton, T.L., N. Dayalani, L.M. Sampaleanu, P.L. Howell & L.L. Burrows, (2015b) Novel
697 role for PilNO in type IV pilus retraction revealed by alignment subcomplex mutations.
698 *J. Bacteriol.* **197**: 2229-2238.

699 Li, W., A. Cowley, U. M., T. Gur, H. McWilliam, S. Squizzato, Y.M. Park, N. Buso & R. Lopez,
700 (2015) The EMBL-EBI bioinformatics web and programmatic tools framework. *Nucl*
701 *Acids Res* **43**(W1): W580-584.

702 Li, X., Mooney, P., Zheng, S., Booth, C.R., Braunfeld, M.B., Gubbens, S., Agard, D.A., and
703 Cheng, Y. (2013). Electron counting and beam-induced motion correction enable
704 near-atomic-resolution single-particle cryo-EM. *Nat Methods* **10**: 584-590.

705 Lopez-Castilla, A., J.-L. Thomassin, B. Bardiaux, W. Zheng, M. Nivaskumar, X. Yu, M.
706 Nilges, E.H. Egelman, N. Izadi-Pruneyre & O. Francetic, (2017) Structure of the
707 calcium-dependent type 2 secretion pseudopilus. *Nat Microbiol* **2**: 1686-1695.

708 Luna Rico, A., J.-L. Thomassin & O. Francetic, (2018) Analysis of bacterial pilus assembly by
709 shearing and immunofluorescence microscopy. *Methods Mol Biol* **1764**: 291-305.

710 Makarova, K.S., E.V. Koonin & S.V. Albers, (2016) Diversity and Evolution of Type IV pili
711 Systems in Archaea. *Frontiers Microbiol* **7**: 667.

712 McCallum, M., S. Tammam, A. Khan, L.L. Burrows & P.L. Howell, (2017) The molecular
713 mechanism of the type IVa pilus motors. *Nat Commun* **8**: 15091.

714 Meibom, K., M. Blokesch, N. Dolganov, C. Wu & G. Schoolnik, (2005) Chitin induces natural
715 competence in *Vibrio cholerae*. *Science* **310**: 1824-1827.

716 Melville, S. & L. Craig, (2013) Type IV pili in Gram-positive bacteria. *Microbiol Mol Biol Rev*
717 **77**: 323-341.

718 Miller, J.H., (1972) *Experiments in molecular genetics*. Cold Spring Harbor Laboratory, Cold
719 Spring Harbor, New York.

720 Mindell, J.A., and Grigorieff, N. (2003). Accurate determination of local defocus and
721 specimen tilt in electron microscopy. *J Struct Biol* **142**: 334-347.

722 Misic, A.M., K.A. Satyshur & K.T. Forest, (2010) *P. aeruginosa* PilT structures with and
723 without nucleotide reveal a dynamic type IV pilus retraction motor. *J Mol Biol* **400**:
724 1011–1021.

725 Monteiro, R., V. Ageorges, M. Rojas-Lopez, H. Schmidt, A. Weiss, Y. Bertin, E. Forano, G.
726 Jubelin, I.R. Henderson, V. Livrelli, A.P. Gobert, R. Rosini, M. Soriani & M. Desvaux,
727 (2016) A secretome view of colonisation factors in Shiga toxin-encoding *Escherichia*
728 *coli* (STEC): from enterohaemorrhagic *E. coli* (EHEC) to related enteropathotypes.
729 *FEMS Microbiol Rev* **363**. pii: fnw179.

730 Ng, D., T. Harn, T. Altindal, S. Kolappan, J.M. Marles, R. Lala, I. Spielman, Y. Gao, C.A.
731 Hauke, G. Kovacicova, Z. Verjee, R.K. Taylor, N. Biais & L. Craig, (2016) The *Vibrio*
732 *cholerae* minor pilin TcpB initiates assembly and retraction of the toxin-coregulated
733 pilus. *PLoS Pathog* **12**. e1006109.

734 Nguyen, Y., S. Sugiman-Marangos, H. Harvey, S.D. Bell, C.L. Charlton, M.S. Junop & L.L.
735 Burrows, (2015) *Pseudomonas aeruginosa* minor pilins prime type IVa pilus assembly
736 and promote surface display of the PilY1 adhesin. *J Biol Chem* **290**: 601-611.

737 Nivaskumar, M., G. Bouvier, M. Campos, N. Nadeau, X. Yu, E.H. Egelman, M. Nilges & O.
738 Francetic, (2014) Distinct docking and stabilization steps of the pseudopilus
739 conformational transition path suggest rotational assembly of type IV pilus-like fibers.
740 *Structure* **22**: 685-696.

741 Nivaskumar, M., J. Santos-Moreno, C. Malosse, N. Nadeau, J. Chamot-Rooke, G. Tran Van
742 Nhieu & O. Francetic, (2016) Pseudopilin residue E5 is essential for recruitment by
743 the type 2 secretion system assembly platform. *Mol Microbiol* **101**: 924-941.

744 Palchevskiy, V. & S.E. Finkel, (2006) *Escherichia coli* competence gene homologs are
745 essential for competitive fitness and the use of DNA as a nutrient. *J Bacteriol* **188**:
746 3902-3910.

747 Parge, H.E., K.T. Forest, M.J. Hickey, D.A. Christensen, E.D. Getzoff & J.A. Tainer, (1995)
748 Structure of the fibre-forming protein pilin at 2.6 Å resolution. *Nature* **378**: 32-38.

749 Pelicic, V., (2008) Type IV pili: e pluribus unum? *Mol Microbiol* **68**: 827-837.

750 Perna, N.T., G.I. Plunkett, V. Burland, B. Mau, J.D. Glasner, D.J. Rose, G.F. Mayhew, P.S.
751 Evans, J. Gregor, H.A. Kirkpatrick, G. Posfai, J. Hackett, S. Klink, A. Boutin, Y. Shao,
752 L. Miller, E.J. Grotbeck, N.W. Davis, A. Lim, E. Dimalanta, K. Potamouisis, J.
753 Apodaca, T.S. Anantharaman, J. Lin, G. Yen, D.C. Schwartz, R.A. Welch & F.R.
754 Blattner, (2001) Genome sequence of enterohemorrhagic *Escherichia coli* O157:H7.
755 *Nature* **409**: 529-533

756 Santos-Moreno, J., A. East, P.J. Bond, G. Tran Van Nhieu & O. Francetic, (2017) Polar N-
757 terminal residues conserved in type 2 secretion pseudopilins determine subunit
758 targeting and membrane extraction during fibre assembly. *J Mol Biol* **429**: 1746-1765.

759 Sauvonnet, N., P. Gounon & A.P. Pugsley, (2000a) PpdD type IV pilin of *Escherichia coli* K-
760 12 can be assembled into pili in *Pseudomonas aeruginosa*. *J Bacteriol* **182**: 848–854.

761 Sauvonnet, N., G. Vignon, A.P. Pugsley & P. Gounon, (2000b) Pilus formation and protein
762 secretion by the same machinery in *Escherichia coli*. *EMBO J* **19**: 2221-2228.

763 Schagger, H. & G. von Jagow, (1987) Tricine-sodium dodecyl sulfate-polyacrylamide gel
764 electrophoresis for the separation of proteins in the range from 1 to 100 kDa. *Anal*
765 *Biochem* **166**: 368-379.

766 Schmidt, H., B. Henkel & H. Karch, (1997) A gene cluster closely related to type II secretion
767 pathway operons of Gram-negative bacteria is located on the large plasmid of
768 enterohemorrhagic *Escherichia coli* O157 strains. *FEMS Microbiol Lett* **148**: 265-272.

769 Seitz, P. & M. Blokesch, (2013) DNA-uptake machinery of naturally competent *Vibrio*
770 *cholerae*. *Proc Natl Acad Sci USA* **110**: 17987-17992.

771 Sievers L, Sievers F, Wilm A, Dineen DG, Gibson TJ, Karplus K, Li W, Lopez R, McWilliam H,
772 Remmert M, Söding J, Thompson JD, & DG, Higgins. (2011) Fast, scalable
773 generation of high-quality protein multiple sequence alignments using Clustal Omega.
774 *Mol Syst Biol* **7**: 539.

775 Sinha, S., A.D.S. Cameron & R. R.J., (2009) Sxy induces a CRP-S regulon in *Escherichia*
776 *coli*. *J Bacteriol* **191**: 5180–5195.

777 Sinha, S. & R.J. Redfield, (2012) Natural DNA uptake by *Escherichia coli*. *PLoS One* **7**:
778 e35620.

779 Sohel, I., J.L. Puente, S.W. Ramer, D. Bieber, C.-Y. Wu & G.K. Schoolnik, (1996)
780 Enteropathogenic *Escherichia coli*: Identification of a gene cluster coding for bundle-
781 forming pilus morphogenesis. *J. Bacteriol.* **178**: 2613-2628.

782 Spaulding, C.N., Schreiber, H.L., Zheng, W., Dodson, K.W., Hazen, J.E., Conover, M.S.,
783 Wang, F., Svenmarker, P., Luna-Rico, A., Francetic, O., Andersson, M., Hultgren, S.,
784 and Egelman, E.H. (2018) Functional role of the type 1 pilus rod structure in
785 mediating host-pathogen interactions. *eLife*. pii e31662.

786 Stone, K.D., H.-Z. Zhang, L.K. Carlson & M.S. Donnenberg, (1996) A cluster of fourteen
787 genes from enteropathogenic *Escherichia coli* is sufficient for the biogenesis of a type
788 IV pilus. *Mol. Microbiol.* **20**: 325-337.

789 Strom, M.S. & S. Lory, (1991) Amino acid substitutions in pilin of *Pseudomonas aeruginosa*.
790 Effect on leader peptide cleavage, amino-terminal methylation, and pilus assembly. *J*
791 *Biol Chem* **266**: 1656-1664.

792 Strom, M.S., D.N. Nunn & S. Lory, (1993) A single bifunctional enzyme, PilD, catalyzes
793 cleavage and N-methylation of proteins belonging to the type IV pilin family. *Proc Natl*
794 *Acad Sci USA* **90**: 2404-2408.

795 Szeto, T.H., A. Dessen & V. Pelicic, (2011) Structure/function analysis of *Neisseria*
796 *meningitidis* PilW, a conserved protein playing multiple roles in type IV pilus biology.
797 *Infect. Immun.* **79**: 3028–3035.

798 Takhar, H.K., K. Kemp, M. Kim, P.L. Howell & L.L. Burrows, (2013) The platform protein is
799 essential for type IV pilus biogenesis. *J Biol Chem* **288**: 740-772.

800 Tammam, S., L.M. Sampaleanu, J. Koo, K. Manoharan, M. Daubaras, L.L. Burrows & P.L.
801 Howell, (2013) PilMNOPQ from the *Pseudomonas aeruginosa* type IV pilus system
802 form a transenvelope protein interaction network that interacts with PilA. *J Bacteriol*
803 **195**: 2126-2135.

804 Tang, G., Peng, L., Baldwin, P.R., Mann, D.S., Jiang, W., Rees, I., and Ludtke, S.J. (2007).
805 EMAN2: an extensible image processing suite for electron microscopy. *J. Struct Biol*
806 **157**: 38-46.

807 Tomich, M., P.J. Planet & D.H. Figurski, (2007) The *tad* locus: postcards from the
808 widespread colonization island. *Nat Rev Microbiol* **5**: 363-375.

809 Veening, J.W. & M. Blokesch, (2017) Interbacterial predation as a strategy for DNA
810 acquisition in naturally competent bacteria. *Nat Rev Microbiol* **15**: 621-629.

811 Wang, F., M. Coureuil, T. Osinski, A. Orlova, T. Altindal, G. Gesbert, X. Nassif, E.H. Egelman
812 & L. Craig, (2017) Cryoelectron microscopy reconstructions of the *Pseudomonas*
813 *aeruginosa* and *Neisseria gonorrhoeae* type IV Pili at sub-nanometer resolution.
814 *Structure.* **25**: 1423-1435.

815 Wolfgang, M., H.-S. Park, S.F. Hayes, J.P.M. van Putten & M. Koomey, (1998) Suppression
816 of an absolute defect in type IV pilus biogenesis by loss-of-function mutations in *pilT*,

817 a twitching motility gene in *Neisseria gonorrhoeae*. *Proc. Natl. Acad. Sci. USA* **95**:
818 14973–14978.

819 Xicohtencatl-Cortes, J., V. Monteiro-Neto, M.A. Ledesma, D. Jordan, O. Francetic, J.B.
820 Kaper, J.L. Puente & J.A. Girón, (2007) Intestinal adherence associated with type IV
821 pili of enterohemorrhagic *Escherichia coli* O157:H7. *J Clin. Investig.* **117**: 3519–3529.

822 Xicohtencatl-Cortes, J., V. Monteiro-Neto, Z. Saldana, M.A. Ledesma, J.L. Puente & J.A.
823 Giron, (2009) The type 4 pili of Enterohemorrhagic *Escherichia coli* O157:H7 are
824 multipurpose structures with pathogenic attributes. *J Bacteriol* **191**: 411-421.

825 Yamamoto, S., H. Izumiya, J. Mitobe, M. Morita, E. Arakawa, M. Ohnishi & H. Watanabe,
826 (2011) Identification of a chitin-induced small RNA that regulates translation of the
827 *tfoX* gene, encoding a positive regulator of natural competence in *Vibrio cholerae*. *J*
828 *Bacteriol* **193**: 1953–1965.

829 Yuen, A.S.W., S. Kolappan, D. Ng & L. Craig, (2013) Structure and secretion of CofJ, a
830 putative colonization factor of enterotoxigenic *Escherichia coli*. *Mol Microbiol* **90**: 898-
831 918.

832
833
834
835
836
837
838
839
840
841 **Table 1. Bacterial strains used in this study**

Name	Genotype	Source/reference
PAP7460	$\Delta(lac-argF)U169 araD139 relA1 rpsL150 \Delta malE444 malG501$ [F' (<i>lacI</i> ^Q $\Delta lacZM15 pro+$ Tn10)]	Laboratory collection
PAP105	$\Delta(lac-pro)$ F' (<i>lacI</i> ^Q $\Delta lacZM15 pro+$ Tn10).	Laboratory collection
BL21	F ⁻ <i>ompT hsdS_B (r_B⁻ m_B⁻) gal dcm</i> (DE3)	Bill Studier
BW25113 F' <i>lacI</i> ^Q	$\Delta(araD-araB)567, \Delta lacZ4787(::rrnB-3), \lambda, rph-1, \Delta(rhaD-rhaB)568, hsdR514$	(Datsenko & Wanner, 2000)
DH5 α F' <i>lacI</i> ^Q	F ⁻ $\Phi 80 lacZ\Delta M15 \Delta(lacZYA-argF) U169 recA1 endA1 hsdR17$ (rK ⁻ , mK ⁺) <i>phoA supE44</i> λ - <i>thi-1 gyrA96 relA1</i>	Laboratory collection
DHT1	Δcya	(Dautin <i>et al.</i> , 2000)

842
843
844
845
846
847
848
849

Table 2. Plasmids used in this study

Name	Origin/ resistance ^a	Relevant markers	Reference
pCHAP8565	p15A/Cm ^R	<i>placZ-ppdD</i>	This study
pSU18	p15A/Cm ^R	multicloning site in <i>lacZ'</i>	(Bartolome <i>et al.</i> , 1991)
pBR322	ColE1/ Ap ^R , Tc ^R	cloning vector	(Bolivar <i>et al.</i> , 1977)
pCHAP8746	p15A/Cm ^R	pSU18 <i>sxy</i>	This study
pCHAP8184	ColE1 / Ap ^R	<i>pulA_{sol}</i> all <i>pul</i> genes Δ <i>pulG</i>	(Campos <i>et al.</i> , 2010)
pCHAP6116	pSC101, Ze ^R	<i>ppdAB-ygdB-ppdC</i>	(Cisneros <i>et al.</i> , 2012b)
pCHAP8889	p15A/Cm ^R	pSU18 <i>hofC</i>	This study
pMS10	ColE1 / Ap ^R	pBR322-cloned <i>ppdD-hofB-hofC</i> , <i>hofMNOPQ</i> and <i>ppdAB-ygdB-ppdC</i> operons flanked by 100 bp of noncoding DNA	This study
pMS37	ColE1 / Ap ^R	<i>ppdD-hofB-hofC</i> , <i>hofMNOPQ</i> and <i>ppdAB-ygdB-ppdC</i>	This study
pMS38	ColE1 / Ap ^R	<i>ppdD-hofB-hofC</i> , <i>hofMNOPQ</i> , <i>ppdAB-ygdB-ppdC</i> and <i>gspO</i>	This study
pMS39	ColE1 / Ap ^R	<i>placZ ppdD-hofB-hofC</i> , <i>hofMNOPQ</i> , <i>ppdAB-ygdB-ppdC</i> and <i>gspO</i>	This study
pMS40	ColE1 / Ap ^R	<i>ppuIC ppdD-hofB-hofC</i> , <i>hofMNOPQ</i> , <i>ppdAB-ygdB-ppdC</i> and <i>gspO</i>	This study
pMS41	ColE1 / Ap ^R	pMS39 Δ <i>ppdD</i>	This study
pMS43	ColE1 / Ap ^R	pMS10 carrying <i>gspO</i>	This study
pMS45	ColE1 / Ap ^R	pMS39 Δ <i>ppdAB-ygdB-ppdC</i>	This study
pMS47	ColE1 / Ap ^R	pMS39 Δ <i>hofC</i>	This study
pUT18c	ColE1 / Ap ^R	<i>placUV5-cyaA</i> T18 fragment in pUC18	(Karimova <i>et al.</i> , 1998)
pKT25	P15A/Km ^R	<i>placUV5-cyaA</i> T25 fragment in pSU38	(Karimova <i>et al.</i> , 1998)
pCHAP8501	ColE1 / Ap ^R	pUT18c- <i>ppdD</i>	This study
pCHAP8504	p15A/Km ^R	pKT25- <i>ppdD</i>	This study
pCHAP8897	ColE1/ Ap ^R	pUT18c- <i>hofB</i>	This study
pCHAP8945	p15A/Km ^R	pKT25- <i>hofB</i>	This study
pCHAP8898	ColE1/ Ap ^R	pUT18c- <i>hofC</i>	This study
pCHAP8899	p15A/Km ^R	pKT25- <i>hofC</i>	This study
pCHAP8907	ColE1/ Ap ^R	pUT18c- <i>hofN</i>	This study
pCHAP8910	p15A/Km ^R	pKT25- <i>hofN</i>	This study
pCHAP8908	ColE1/ Ap ^R	pUT18c- <i>hofO</i>	This study
pCHAP8911	p15A/Km ^R	pKT25- <i>hofO</i>	This study
pCHAP8909	ColE1/ Ap ^R	pUT18c- <i>hofP</i>	This study
pCHAP8912	p15A/Km ^R	pKT25- <i>hofP</i>	This study
pMS30	ColE1/ Ap ^R	pUT18c- <i>ppdB</i>	This study
pMS26	p15A/Km ^R	pKT25- <i>ppdB</i>	This study
pCHAP8246	ColE1/Ap ^R	pUT18c- <i>pulJ</i>	(Cisneros <i>et al.</i> , 2012a)
pCHAP8364	ColE1/Ap ^R	pUT18c- <i>pulF</i>	(Nivaskumar <i>et al.</i> , 2016)

pCHAP7330	ColE1/Ap ^R	pUT18c- <i>pulG</i>	(Nivaskumar <i>et al.</i> , 2014)
pCHAP7332	P15A/Km ^R	pKT25- <i>pulG</i>	(Nivaskumar <i>et al.</i> , 2014)
pCHAP8154	ColE1/Ap ^R	pUT18c- <i>pulM</i>	(Nivaskumar <i>et al.</i> , 2016)
pCHAP8113	ColE1/Ap ^R	pUT18c- <i>pulC</i>	(Nivaskumar <i>et al.</i> , 2016)
pCHAP8256	ColE1/Ap ^R	pUT18c- <i>pulH</i>	(Nivaskumar <i>et al.</i> , 2016)
pCHAP8472	ColE1/Ap ^R	pUT18c- <i>pulL</i>	(Nivaskumar <i>et al.</i> , 2016)

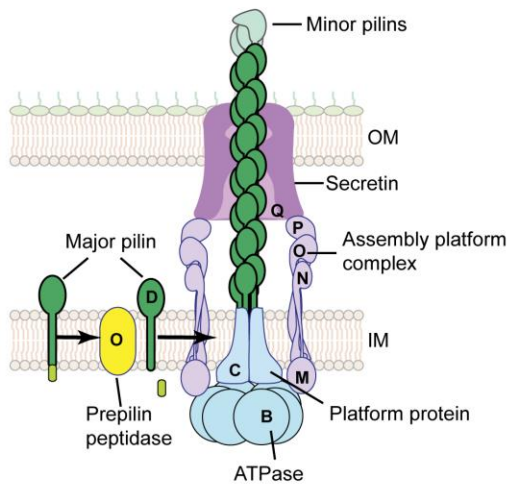
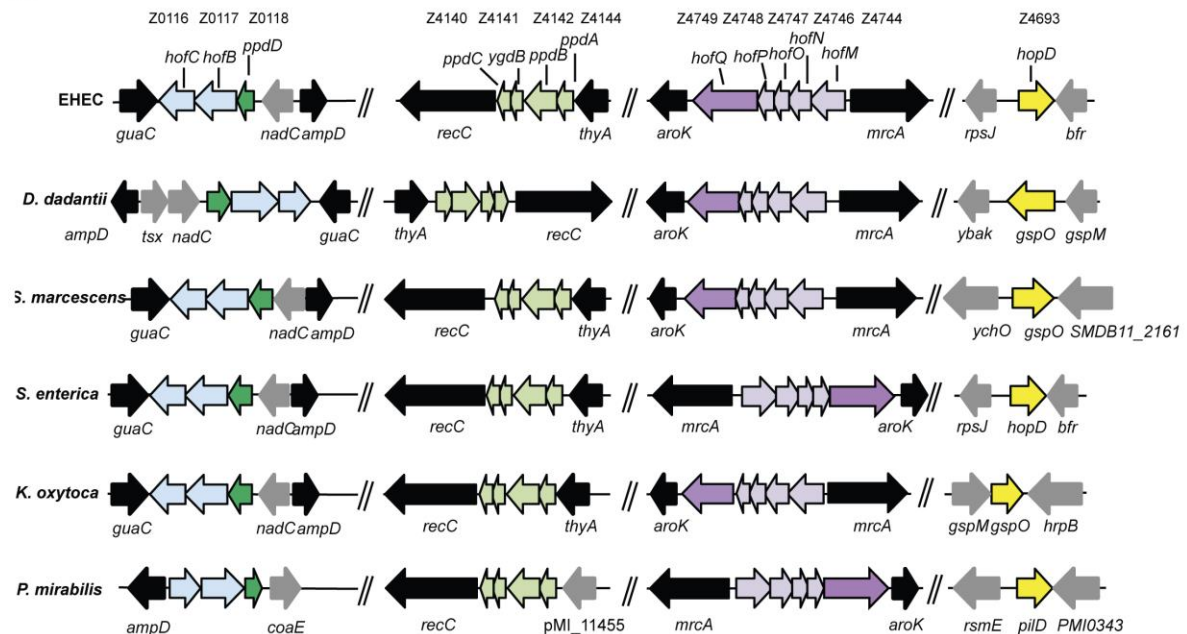
852 a. Ap, ampicillin; Cm, chloramphenicol; Km, kanamycin; Ze, zeocin.

853

854 **Table 3. Comparison of helical symmetry parameters among bacterial pili of the Tff**
855 **superfamily.**

Pili	Rise (Å)	Twist (°)
<i>Neisseria meningitidis</i> type 4a pili	10.3	100.8
<i>Neisseria gonorrhoeae</i> type 4a pili	10.1	100.8
<i>Pseudomonas aeruginosa</i> type 4a pili	10.5	87.3
<i>Escherichia coli</i> type 4a pili	11.2	96.0
<i>Klebsiella oxytoca</i> T2SS pseudopili	10.2	83.2

856

A**B**

858

859

860

861

862

863

864

865

866

867

868

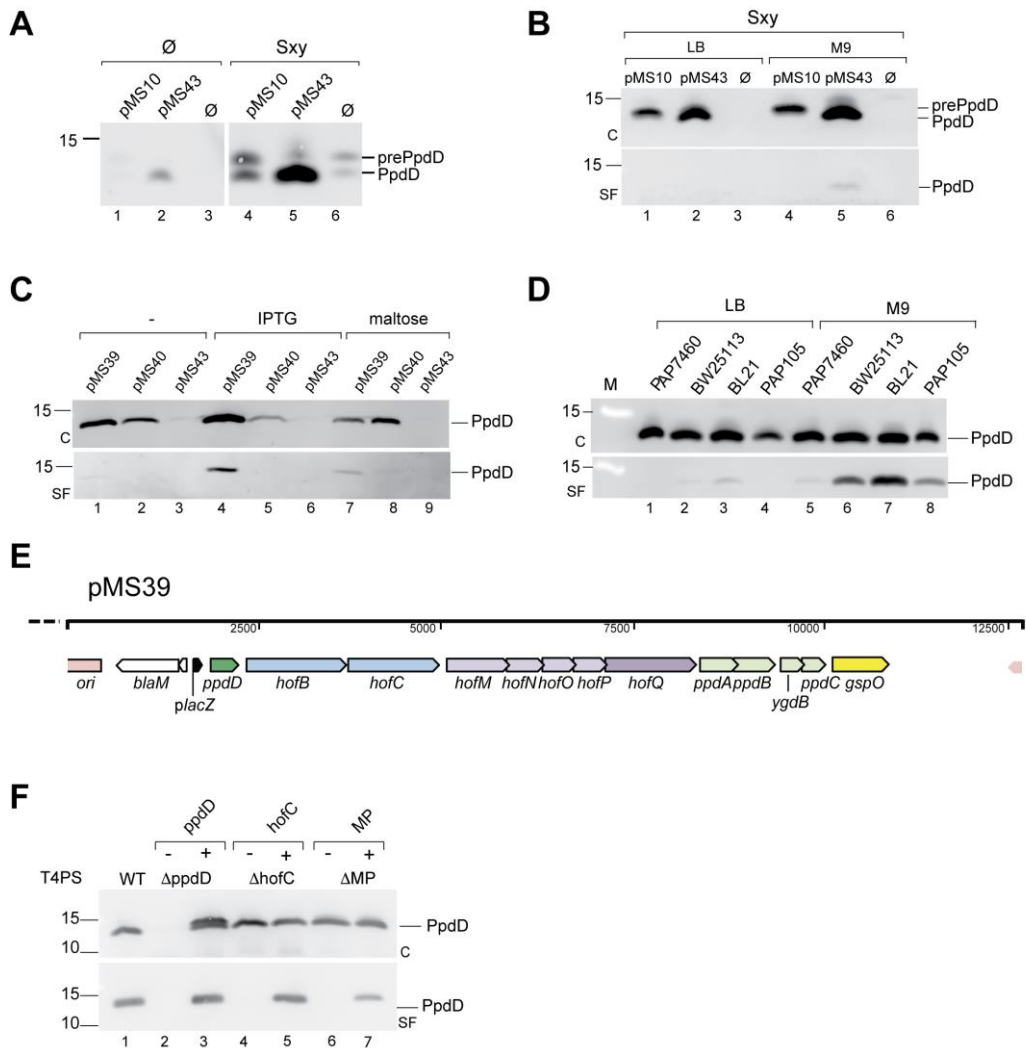
869

870

871

Figure 1. The T4aP assembly systems. **A**, Schematic representation of the T4aP assembly system in the Gram-negative bacterial envelope. Major (D, dark green) and minor pilins (in light green) are processed by the prepilin peptidase (O, yellow). Cytoplasmic ATPase (B) transmits conformational changes to the inner membrane (IM) platform protein (C) and the assembly complex M-N-O-P (light purple), which is connected with the secretin (Q, dark purple) in the outer membrane (OM). **B**, Organization of T4aP gene clusters in EDL933 genome (EHEC) and in the representative species of the order of Enterobacteriaceae: *Dickeya dadantii*, *Serratia marcescens*, *Salmonella enterica*, *Klebsiella oxytoca* and *Proteus mirabilis*. The *ppd-hof* genes are indicated as arrows whose length represents relative gene size, colour-coded as in Fig. 1A. Genes adjacent to T4P clusters are represented as black and grey arrows reflecting relative degree of conservation. For EHEC, annotation numbers are indicated above each T4P gene in blue.

873 **Figure 2.** Protein sequence alignments of major pilin subunits. **A**, Multiple alignment of
874 major T4a pilin sequences from diverse Enterobacterial strains: EHEC (WP_000360900.1),
875 *E. coli* K-12 (WP_000360904.1), *Citrobacter werkmanii* (WP_042312306.1), *Klebsiella*
876 *oxytoca* (WP_064398298.1), *Salmonella enterica* (WP_061382948.1), *Shigella dysenteriae*
877 (WP_000360691.1), *Proteus mirabilis* (WP_060558290.1), *Morganella morganii*
878 (WP_064483293.1), *Edwardsiella tarda* (WP_005282704.1), *Serratia marcescens*
879 (WP_060440768.1), *Brenneria sp.* (WP_009111461.1), *Raoultella terrigena*
880 (WP_045859871.1), *Kluyvera ascorbata* (WP_035893064.1), *Pantoea theicola*
881 (WP_103059883.1), *Erwinia toletana* (WP_017800450.1), *Trabulsiella odontotermitis*
882 (WP_049856566.1), *Dickeya dadantii* (WP_038923864.1), *Yersinia enterocolitica*
883 (WP_046695439.1), *Xenorhabdus nematophila* (WP_010845542.1) and *Photorhabdus*
884 *luminescens* (WP_011147801.1). The arrowhead indicates the prepilin peptidase cleavage
885 site upstream of the N-terminal F1 residue of mature pilins. **B**, Pairwise alignment of *P.*
886 *aeruginosa* PilA and *N. gonorrhoeae* PilE. Alignments showing identical (*), conserved (:)
887 and similar (.) residues were performed with Clustal omega (Sievers *et al.*, 2011) and the
888 EMBL-EBI tools (Li *et al.*, 2015). Conserved Cys residues are highlighted in bold with orange
889 background; putative disulphide bridges are indicated above. Hydrophobic (light grey), Pro
890 (dark grey), Gly (white), polar (green), aromatic (yellow), negatively (pink) and positively
891 charged (blue) residues are indicated.
892



894

895

Figure 3. Construction, optimization and complementation analysis of the synthetic *ppd-hof*

operon. **A**, The Sxy-mediated induction of *ppdD* expression in *E. coli* strain PAP7460

carrying pMS10, pMS43 and pBR322, without (Ø) or with *sxy* gene on plasmid pCHAP8746.

Total extracts from 0.15 OD_{600nm} of bacteria cultured on LB plates containing IPTG for 48

hours were analysed by SDS-PAGE and immunodetection using anti-PpdD antibodies

(1:1000); **B**, Bacteria of strain PAP7460 containing plasmid pCHAP8746 and either pMS10,

pMS43 or vector pBR322 (Ø) cultured on LB or M9-glycerol media for 48 hours. Pilus

assembly was assayed as described in Experimental procedures. C, cell fraction; SF,

sheared fraction; M, molecular weight marker. **C**, Construct optimization. Pilus assembly in

strain PAP7460 containing plasmid pMS43, compared with optimized constructs pMS39 and

pMS40 cultured in LB (-) or LB containing IPTG or maltose as inducers. **D**, Pilus assembly in

indicated *E. coli* host strains transformed with plasmid pMS39 and cultured on selective LB

or M9 glycerol plates containing IPTG. **E**, Linear map of the pMS39 construct with an artificial

ppd-hof operon under *placZ* control. Gene names are indicated and colour-coded

corresponding to the scheme in Fig. 1A. **F**, PpdD pilus assembly in pMS39 (WT) and its

deletion derivatives lacking *ppdD* (pMS41), *hofC* (pMS47) and minor pilin (MP) *ppdAB-ygdB-*

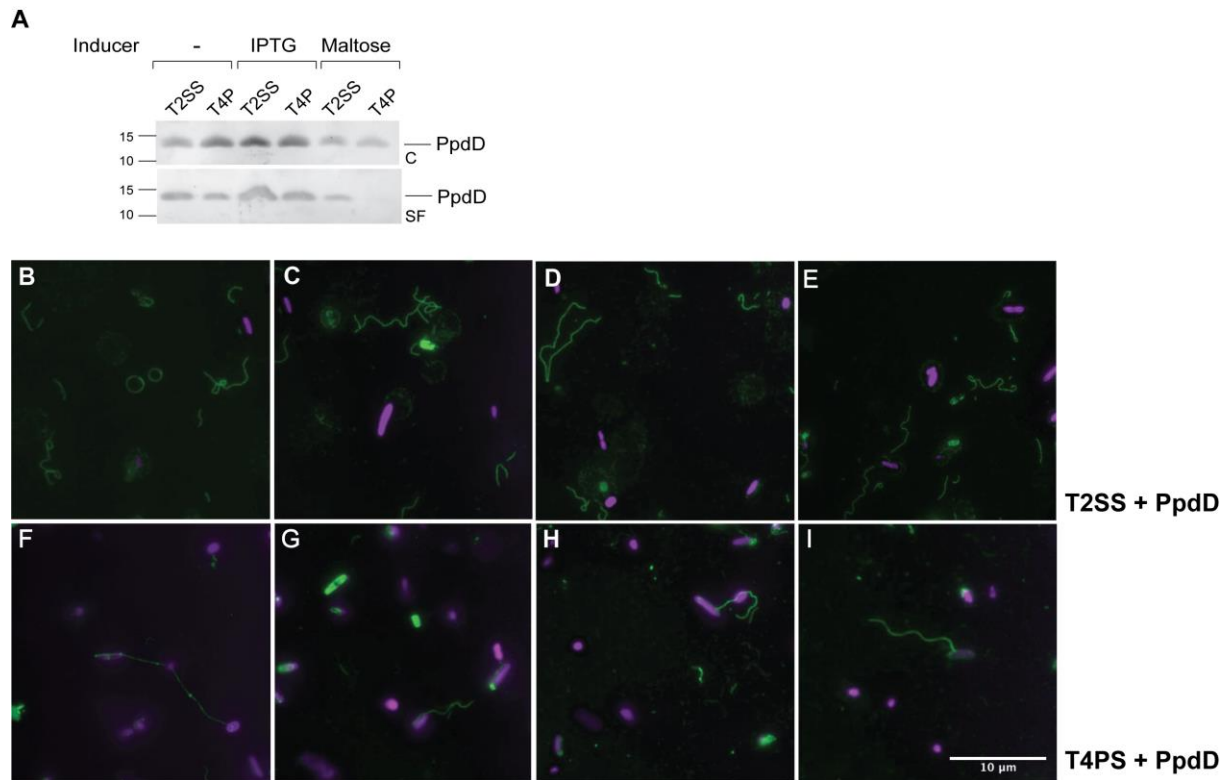
ppdC genes (pMS45). Strain BW25113 F'*lacI*^Q containing complementing plasmids (+) of

empty vector (-) were grown on selective M9 glycerol plates containing IPTG. In Panels B, C

and F samples of cell (C) and sheared fractions (SF) from 0.05 OD_{600nm} equivalents were

analysed by SDS-PAGE and immunoblot with anti-PpdD antibodies diluted 1:2000.

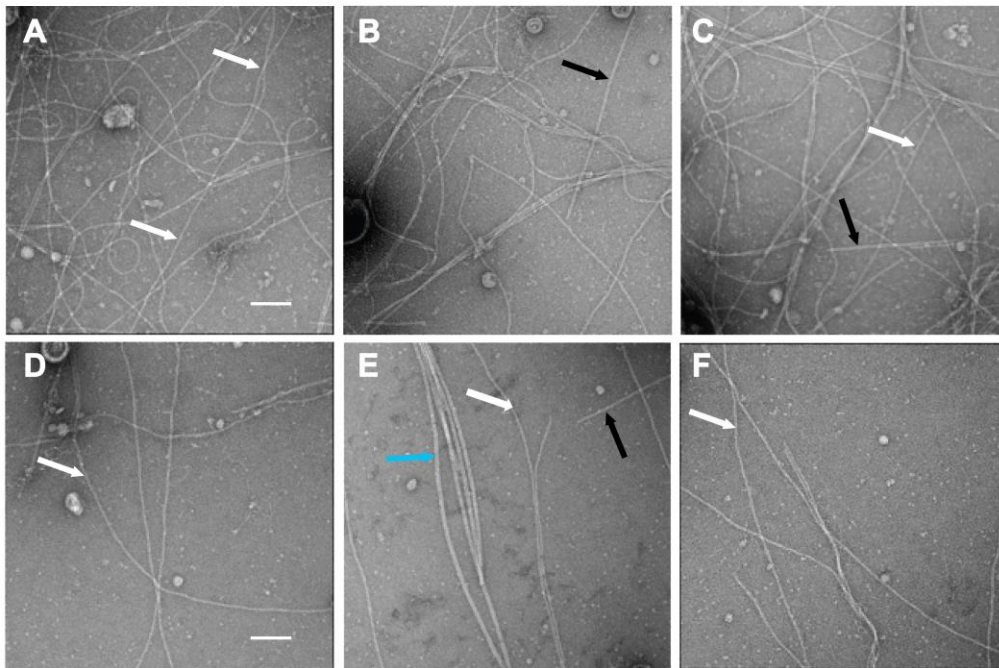
894



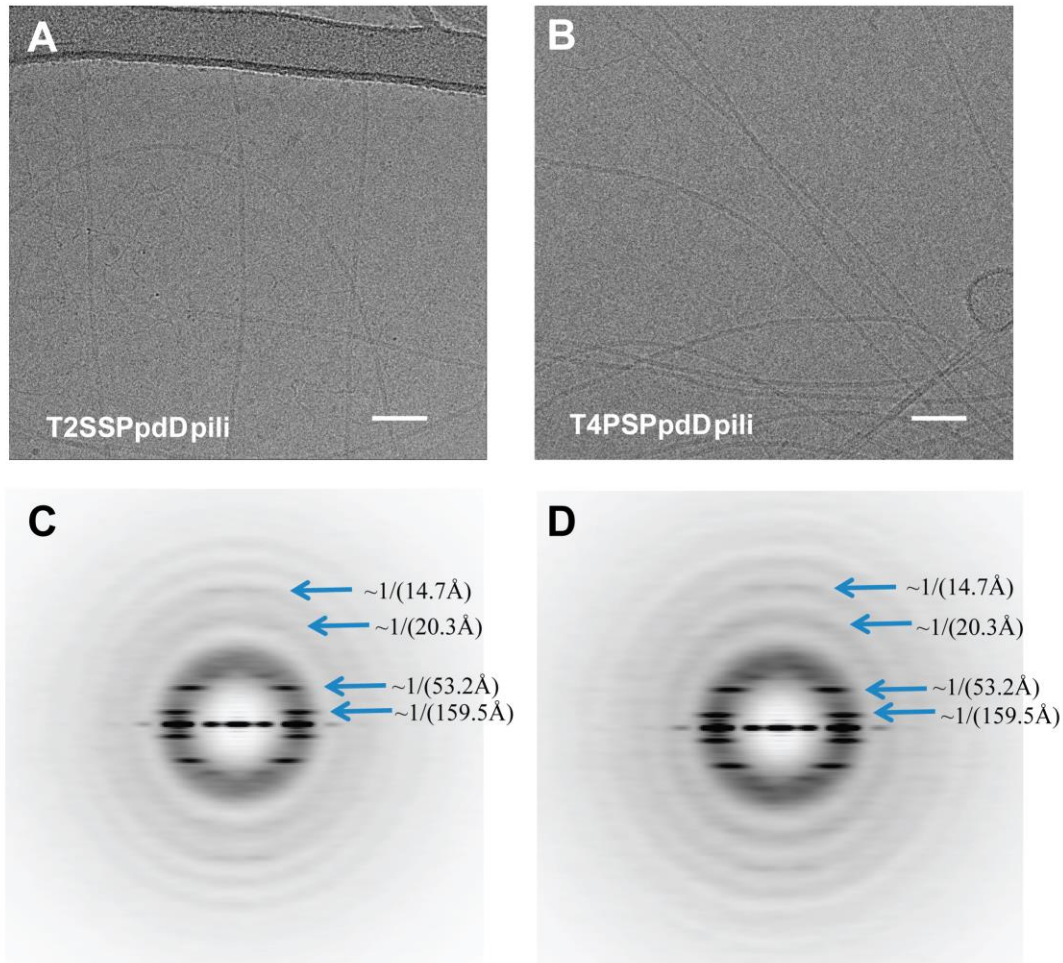
915

916 **Figure 4.** Comparison of PpdD pilus assembly *via* the T2SS and T4PS. **A**, *E. coli* strain
 917 BW25113 $F'lacI^Q$ containing plasmid pCHAP8565 and pCHAP8184 (T2SS) or pMS41
 918 (T4PS) was grown on LB plates containing AP and Cm at 30°C for 48 hours, without or with
 919 indicated inducers. Fractionation and Western blot with antibodies raised against MalE-PpdD
 920 fusion protein were performed as described in Experimental procedures. Migration of
 921 molecular weight markers is indicated on the left. **B-E**, Immunofluorescence microscopy
 922 analysis of PpdD pili assembled by the T2SS or by the T4PS (**F-I**). Samples were processed
 923 as indicated in Experimental procedures. Pili are labelled in green (GFP) and bacterial
 924 nucleoid in magenta (DAPI). Scale bar indicates 10 μ M.
 925

926

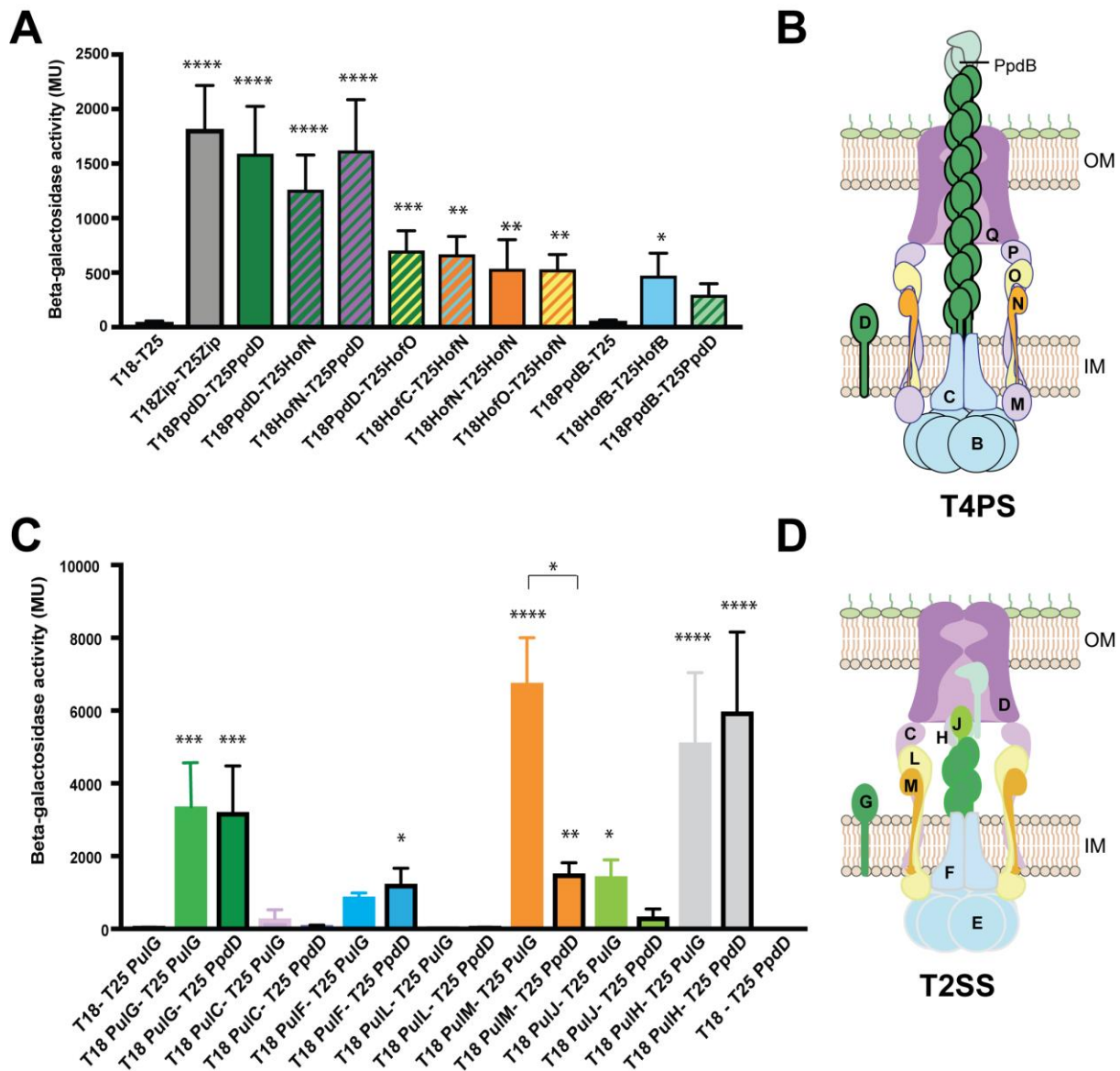


927
 928 **Figure 5.** Negative staining electron microscopy PpdD pili assembled by T4PS and T2SS.
 929 Crude sheared fractions of strains BW25113 F' expressing *ppdD* (from pCHAP8565) and
 930 either the T2SS genes (from pCHAP8184) (panels A-C) or T4PS genes (from pMS41)
 931 (panels D-F) were analysed. Black arrows indicate Type 1 pili (in panels B and C) as shown
 932 previously in (Spaulding *et al.*, 2018), the blue arrow indicates flagella (in panel E) and white
 933 arrows indicate PpdD T4P. The scale bar (A) is 50 nm.
 934



935
 936 **Figure 6.** PpdD pili assembled by the *Klebsiella* Pul T2SS and EHEC T4SP show similar
 937 architecture and helical symmetry. Representative cryoEM images of PpdD pili from T2SS
 938 (A) and T4PS (B). Scale bar, 50 nm. The helical symmetry of PpdD pili from T2SS (C) and
 939 T4PS (D) were determined by the averaged power spectra generated from 384-pixel long
 940 segments. Due to the variability of both twist and axial rise in the PpdD filaments, sorting by
 941 helical symmetry generates improved power spectra. The power spectra in (C) and (D) were from
 942 the ~25% of segments classified as having a twist near 96° and a rise near 10.8 Å. The blue
 943 arrows indicate the dominant layer lines.
 944

945



946
947
948
949
950
951
952
953
954
955
956
957
958
959
960
961
962
963

Figure 7. PpdD interactions with components of the T4PS and T2SSs. **A**, BAC2H analysis of interactions between PpdD and T4PS components, performed as described in Experimental procedures. Bar graphs represent mean β -galactosidase activities (in Miller units) measured from at least 6 independent co-transformants; error bars indicate standard deviation. Statistical analysis with ANOVA test in comparison with the negative control with significant probabilities indicated above bars: ****, $p < 0.0001$, *** $p < 0.001$, **, $p < 0.01$; *, $p < 0.01$. **B**, Cartoon model of the T4PS with different Hof -Ppd components indicated in single letter code (except PpdB, to avoid confusion with HofB), colour-coded corresponding to the bar graphs in (A). **C**, Bar graphs show mean β -galactosidase activities in a BAC2H assays, comparing interactions of T25-PulG (no contours) and T25-PpdD (black contours) with T18-fused T2SS components. Statistical analysis was performed with ANOVA test in comparison with the negative control. Significant probabilities (when applicable) are indicated above bars: ****, $p < 0.0001$, *** $p < 0.001$, **, $p < 0.01$; *, $p < 0.01$. Non-parametric Kruskal-Wallis and Dunn's multiple comparison between pair groups identified a significantly lower degree of interaction between PulM-PpdD when compared to PulM-PulG. **D**, Cartoon model of the Pul T2SS with different Pul components indicated in single-letter code and colour-coded as in (C).